Emission lines in the long period Cepheid ℓCarinae

Erika Böhm-Vitense and Stanley G. Love

Astronomy Department, University of Washington, Seattle, WA 98195

Abstract

For the Cepheid ℓCarinae with a pulsation period of 35.5 days we have studied the emission line fluxes as a function of pulsational phase in order to find out whether we see chromospheric and transition layer emission or whether we see emission due to an outward moving shock. All emission lines show a steep increase in flux shortly before maximum light suggestive of a shock moving through the surface layers. The large ratio of the CIV to CII line fluxes shows that these are not transition layer lines.

During maximum light the large ratio of the CIV to CII line fluxes also suggests that we see emission from a shock with velocities >100km/sec such that CIV emission can be excited.

With such velocities mass outflow appears possible.

The variations seen in the MgII line profiles show that there is an external absorption over a broad velocity band independent of the pulsational phase. We attribute this absorption to a circumstellar "shell". This "shell" appears to be seen also as spatially extended emission in the OI line at 1300 Å, which is probably excited by resonance with Lyβ.

1. Introduction

The long period Cepheid ℓCarinae was observed extensively in the UV by Schmidt and Parsons (1982) in order to study the dependence of the UV emission line fluxes on the pulsational phase. They found that the star showed rather strong emission in the OI lines at all phases for which they observed it. The OI line was always the strongest emission line and

becomes especially strong during rising light. At this phase emission lines of SiII, CII, and CIV were also visible. Observations shortly before this phase were missing in their study.

The reason for the occurrence of the emission is not clear. Schmidt and Parsons concluded that the emission is due to an outward moving shock while Böhm-Vitense and Querci (1988) suggested that it is due to the development of an effective convection zone during phases of low temperature and minimum light, leading to a build up of a stellar chromosphere, transition layer, and possibly corona.

If the high ionization emission lines are due to an outward progressing shock we expect the high ionization lines to appear first. The lower ionization lines appear later in the post shock region where the gas cools down. The timescale of the delay depends on the cooling time, which in turn depends on the density. It could be very short. In any case if the emission is due to a shock we would not expect the CII emission to occur before the CIV emission.

On the other hand, ℓCarinae is at the red edge of the Cepheid instability strip. We may therefore expect convection to develop during the cool phases, leading to the production of mechanical energy flux which heats up the outer layers of the atmosphere, forming a chromosphere and transition layer. If so we expect the low ionization lines to appear first. Especially the CII lines are expected to appear before the CIV lines because the CIV lines will only occur when temperatures around 10^5 K are reached. The time difference between the occurrence of these two lines is determined by the time required for the mechanical flux to supply enough energy to heat the outer layers from 20,000 K to about 100,000 K. While this time is hard to estimate, we expect time delays less than of a tenth of a period. We expect the lower ionization lines to fade later than the CIV lines as is the case for shock generated emission.

In order to get more information about the origin of the emission lines in this long period Cepheid we obtained new observations to study the phase dependence of the emission

line fluxes and especially the phase dependence of the CII/CIV emission line flux ratio. We suspected that convection might have developed for phases around 0.6. We therefore concentrated our observations near phase 0.6 and extended them to phases near 0.8. Several interesting results were obtained from the new and the archival data especially for the MgII and OI line emission.

2. The Observations

2.1. Available IUE Data

In Table 1a we list the available IUE (International Ultraviolet Explorer Satellite) observations for both wavelength regions: the long wavelengths region, 2000-3100 Å, and the short wavelength region, 1150-2000 Å. Observations for the short wavelength region have low resolution ($\Delta\lambda/\lambda = 300$), for the long wavelength region there are high ($\Delta\lambda/\lambda = 10,000$) and low resolution spectra.

In Table 1a we also list the pulsational phases for the observations calculated according to the ephemeries given by Schmidt and Parsons (1982). Also listed are the FES (Fine error sensor) photon counts obtained at the IUE observatory to measure the visual apparent magnitudes of the Cepheid generally with an error of $\pm$ 0.1. One has to keep in mind, however, that the reflectivity at the reference point, at which the photons are counted, has decreased with time. The recent counts have to be increased by about 20% in order to compare them with the earlier counts. We also give the roll angles of the spacecraft, which determines the orientation of the large aperture (10" $\times$ 20"). This enables us to determine in which direction spatially extended emission is seen, if there is any. For most observations the aperture orientation was around $294° \pm 13°$. This means if spatially extended emission is seen coming from the same place in the sky it is expected to occur at nearly the same offset from the stellar spectrum.

From Table 1 it is obvious that the spectra are grouped in time, the earlier set taken

in 1980 by Schmidt and Parsons and the later ones in 1988 which were taken by us. There are only a few spectra taken by other observers. The earlier spectra were usually taken with rather short exposure times. There are only two earlier long exposure spectra available taken by L.A. Willson.

2.2. The Spectra

In Figure 1a we have plotted the FES (visual) photon counts as a function of phase on a logarithmic scale. For phases of maximum light the effect of the decreasing reflectivity of the face plate at the reference point between 1980 and 1988 is seen which reduces the counts for 1988 by about 20% with respect to those of 1980. This effect is less obvious for minimum light because no observations were taken for those phases in 1980.

In the Figure 1b we have plotted the radial velocities as a function of phase as measured by Stibbs (1955).

In Figure 2 we show the short wavelength, low resolution spectra as a function of phase including the observations by Schmidt and Parsons. The OI line at 1300 Å is usually quite strong, and is always measurable. Several satellite lines are seen mainly on the short wavelength side. The next strongest line is the SiII line at 1817 Å. The HeII line at 1640 Å is frequently seen though it is generally quite weak. The CIV line is seen only between phases 0.9 and 1. The CII line is surprisingly weak at these phases. It is invisible at other phases.

In Figure 3 we show the Mg II high resolution line profiles as a function of velocity. The profiles are shown in succession of pulsational phase. Rather striking variations are seen in the profiles which we will discuss in detail in section III.

In Figure 4 we have plotted the observed emission line fluxes for the CIV and the OI lines as a function of pulsational phase (uncorrected for the sensitivity change of the camera. The corrections are $\lesssim$10% and are smaller than the uncertainties in the measurements). For the earlier observations the fluxes were given by Schmidt and Parsons. For overlapping phases

the 1980 measurements match well with the 1988 measurements.

In Figure 5 we have plotted the OI line profiles as a function of wavelength. The line is frequently very broad and may include contributions from other lines which vary in intensity. We will come back to this problem section V. In Figure 4 we have given the fluxes for the whole broad feature. These fluxes vary smoothly, rather similar to the light curve except that the increase in the flux of the OI line occurs somewhat later than in the visual light and in the CIV lines, which reach a maximum before the visual light maximum.

For the CIV fluxes we see an abrupt increase for phases > 0.8 and reaching a maximum at phase 0.95, which means somewhat earlier than the phase at which the visual magnitude and the OI lines reach their maximum.

A second maximum in the CIV line fluxes possibly may occur around phase 0.3, but so far it is indicated by only two measurements. More observations will be needed to be certain.(At this phase a small bump in the light curve may be indicated). At other phases the CIV emission is weak or absent. Only upper limits for the flux can be given.

In Table 2 we give the measured fluxes for the OI, CII and CIV lines. The uncertainties are at least 20%. The CII lines are generally very weak or absent. Some CII emission can, however, be measured for phases around maximum CIV line fluxes.

3. Transition layer or shock wave emission?

Since observations between phases 0.8 and 0.9 are missing we cannot decide whether CII or CIV line emission starts earlier. At phase 0.912 some CIV emission line flux can be measured. If present at all the CII line flux is too weak to be measurable.

In solar type transition layers, the CIV line fluxes are usually larger than the CII line fluxes by a factor between 1.5 to 3. For phases of large CIV line flux the CIV to CII line flux ratio in ℓCarinae is clearly much larger than seen in solar type transition layers. (The correction for interstellar absorption corresponding to E(B-V) = 0.16 reduces the carbon

line flux ratio by only 20%.) This seems to indicate that at these phases we are not looking at the emission of a solar type transition region layer but rather at a shock with velocities >100 km/sec such that carbon can be ionized to CIV which requires 47.9 eV. We thus reach the same conclusion as Schmidt and Parsons: At phases around maximum light the emission lines originate in an outwards propagating shock.

The emission of the CIV line, if due to a shock, requires velocities $\geq$100 km/sec. These are necessary to achieve such high degree of ionization. We thus know that velocities $\geq$ 100 km/sec must be present in the shock. The escape velocity for ℓCarinae is also of the order of 100 km/sec if we accept M = 5 $M_\odot$ and R=140 $R_\odot$ (Böhm-Vitense *et al.* 1989). This opens the possibility of mass loss and of circumstellar material around ℓCarinae, which we think we see in the MgII lines and in the O I lines.

4. The Mg II lines

4.1. The line profiles

The MgII lines in ℓCarinae were first studied by Schmidt and Parsons (1982). They had only a few high resolution spectra around maximum light. Their discussion could therefore be only preliminary. They found a broad central absorption in these lines, possibly due to two overlapping components, which they attributed to either interstellar or circumstellar absorption or both. (From the study of the H_α absorption components Rogers and Bell (1965) also suspected circumstellar absorption in that line). Schmidt and Parsons also found a strong increase in the MgII emission at phases before maximum light. The total surface flux observed for these phases was similar to the fluxes observed for the chromospheric emission of non-pulsating stars of luminosity class II. Nevertheless they suspected that at least part of the emission was due to an outwards propagating shock.

We now have a much larger phase coverage with high resolution spectra, which enables us to do a more detailed study and especially to derive more information about the circumstellar gas.

In Figure 3 we have shown line profiles of the MgII h and k lines as a function of wavelength expressed in velocities corresponding to $\Delta\lambda$ from the line centers as given in the Figures. A broad central absorption is always prominent dividing the lines into a "blue" and a "red" part. In the emission lines several bumps and dips are seen. If real absorption or emission line components occur for a given velocity they should show up in both lines. Several bumps and dips are indeed seen in both lines. Perhaps we see gas masses ejected in different pulsation cycles traveling with different velocities. In the k lines some dips could be due to absorption in Mn I lines at 2794.817 Å (−76 km/sec), 2798.270 Å (+294 km/sec) and in the Fe I line at 2795.006 Å (−56 km/sec). In the h line the MnI line at 2801.084 Å (−173 km/sec) and the FeI line at 2803.169 Å (+49 km/sec) could be present. (See Bernat and Lambert 1976.) Dips at these wavelengths may be seen at some phases but not at others.

The broad central absorption remains essentially unchanged during the pulsational cycle in the otherwise changing line profiles. This absorption appears to consist of two overlapping components unless there is a weak emission line in the center of the broad absorption. The two absorption components appear to have a velocity difference of about 30 km/sec. Since they remain unchanged during the pulsation cycle they must be caused by interstellar or circumstellar absorption. (Rodgers and Bell observed an Hα absorption component which also remained at constant velocity, which they also attributed to circumstellar gas). These strong Mg II absorption components then again point to circumstellar gas around ℓCarinae. We probably see evidence of mass loss.

In Table 3 we give the peak fluxes of the "blue" and the "red" wings seen at about ±75 km/sec for the k and h lines.

The profiles of the emission lines change from stronger "blue" wings for phases $0.7<P<1.1$ to stronger "red" wings for phase $0.1<P<0.65$. In Figures 6 and 7 we have plotted as a function of phase the peak intensities for the "blue" wings and the "red" wings, seen at −75 km/sec and at +75 km/sec during minimum light phases. During phases of minimum

light we see a smooth increase in flux for both wings, with the "blue" wing being the weaker one. This slow increase might possibly be due to the formation of a chromosphere due to the slow onset of convection, though we do not know. Then at phases between 0.8 and 0.9 a very steep increase in flux occurs, supposedly due to an outwards propagating shock (see also Schmidt and Parsons 1982). The increase in the "blue" wing is much stronger than in the "red" wing. Additional emission occurs mainly in the "blue" wing at velocities between 75 km/sec and −250 km/sec. The increase in the "red" wing of the Mg II lines during phases of the outwards moving shock must be due to either an increasing source function for a broad underlying emission originating in deeper layers, or due to outwards moving gas on the "back side" of the star if the radius of the emitting shock is much larger than the photosphere. Since the increase in the "red" wing occurs also at rather large velocities this latter possibility requires a rather large extent for the shocked layer. During phases of maximum light the peak flux for the "red" wing occurs at velocities around 100 to 125 km/sec. The velocity is larger for the k line, showing that the shift is probably due to a redward shifted central absorption, which is stronger in the k line than in the h line.

Once the shock has propagated and expanded the MgII emission decays quickly though not as fast as the CIV emission as can be seen in Figure 4. The MgII lines are still emitted in the cooling region behind the shock, while the high ionization lines have decayed already together with the high temperature shock.

4.2. Comparison of the h and k line peaks

In Figure 8 we compare the phase dependance of the h and k line peak fluxes in the "blue" wings. During minimum light phases the h line is the stronger line while after the sudden increase in emission the k line is the stronger one. Theoretically the h line at 2802.7 Å is expected to be the weaker line. The gf value is smaller by a factor of 2 than the gf value for the 2795.5 Å k line. The observed larger flux in the h line during minimum light phases can only be due to stronger overlying absorption in the k line. The strength of this

absorption can be estimated in the following way:

If the Mg II emission occurs in an optically thick layer then the peak fluxes in the h and k line wings at a given velocity could be equal. For smaller optical depth the k line flux should be larger. Assuming equal flux gives us the highest possible h line flux and thereby a minimum value for the overlying absorption. We compare fluxes at the velocity of -75 km/sec, the peak fluxes. For equal intrinsic fluxes f_i (emitted before subject to external absorption) in the h and k lines we must have

$$f_i(k) = f(k)e^{\tau(k)} = f(h)e^{\tau(k)/2} = f_i(h)\,. \tag{1}$$

Here we have made use of the fact that the optical depth $\tau(h) = 1/2\ \tau(k)$, the latter being the optical depth in the k line at -75 km/sec. The f(h) and f(k) are the observed fluxes in the h and k lines at -75 km/sec. We then find

$$f(k)/f(h) = e^{-\tau(k)/2}\,. \tag{2}$$

At phase 0.65 the observed flux ratio is 0.75. We thus find $\tau(k,\ -75\ \mathrm{km/sec}) \leq 0.64$.

For the "red" wing, see Figure 9, we find for v = 75 km/sec that the fluxes in the h and k line are essentially equal for phases near minimum light. This means *if* $f_i(k) = f_i(h)$ then there is no external absorption for this velocity. The "red" wing may, however, be less optically thick than the "blue" wing. In this case the $\tau(k, 75\mathrm{km/sec})$ could be larger than 0. Using the observed fluxes for phase 0.75 we find $\tau(k, -75\ \mathrm{km/sec}) \geq 0.62$. If we use this optical depth also for the red wing we find for the ratio of the intrinsic fluxes $f_i(k)/f_i(h) = 1.34$ corresponding to an intrinsic optical depth of the emitting layer of about 2 for the k line in the red wing for a velocity of 75 km/sec.

We now turn to the phases around maximum light, after the shock has passed through the surface layers. At maximum flux we find for the "blue" wing that the h line is again stronger than the k line. The k line then decreases more slowly than the h line, showing that the k line was at maximum light intrinsically more optically thick than the h line but

becomes less optically thick. For phases >0.1 the line fluxes in the two lines decrease in parallel, which means they are of nearly the same intrinsic optical depth. Now the k line flux is larger than the h line flux which indicates close to optically thin emission. For strictly optically thin emission the fluxes at a given velocity should be $f_i(k) = 2f_i(h)$, which means

$$f(k) = f_i(k)e^{-\tau(k)} \text{ and } f(h) = f_i(h)e^{-\tau(k)/2} = 1/2\ f_i(k)e^{-\tau(k)/2} \quad (3)$$

The ratio f(k)/f(h) becomes

$$f(k)/f(h) = 2e^{-\tau(k)/2} \quad (4)$$

With the observed value for phase 0.05 and v = −75 km/sec we find τ(k, −75 km sec) = 0.82 or less if the lines are not strictly optically thin at this phase. At phase 0.15 we find τ(k, −75 km/sec) = 0.62. For this velocity we thus find the same overlying absorption for different phases with very different line flux ratios. We are most probably dealing with a shell surrounding the star at distances at which the velocities are essentially not influenced by the pulsation.

For the "red" wing we find for the phase 0.05 that τ(k, 110 km/sec) = 0.97, and for phase 0.25 the τ(k, 90km/sec) = 0.59. We find again that right after maximum flux the line is intrinsically not yet optically thin but shortly thereafter it becomes optically thin at this velocity.

Considering the stronger central absorption which reduces the k line peak flux more than the h line peak we should actually use a larger f(h)/f(k) peak flux ratio. This will lead to a smaller value for τ. For phase 0.25 the peak flux for the k line still occurs at somewhat larger velocities than for the h line, but the difference is smaller. Both occur around 90 km/sec. We may guess that the effect of the central absorption is reduced. For this phase we find from the measured ratio of the peak fluxes that τ(k, $\sim$ 90 km/sec) = 0.59, which is an upper limit for τ at this velocity and phase.

Using the optical depth of τ(k, −75 km/sec) = 0.65 ± 0.1 we can then estimate the column density for the absorbing "shell". For the determination of the optical depth for v=0

we have to know the Doppler width, which means we have to know the turbulent velocity. If we assume that the broad central absorption seen in the MgII line profiles is due to the same "shell", then the equivalent width of this absorption can give us an estimate for the Doppler width. From the curve of growth we find that the equivalent width $W_\lambda \sim -\log\alpha$ (see Unsöld 1955). Here $\alpha = \gamma/(2\Delta\omega_D)$, where γ is the damping constant and $\Delta\omega_D$ is the Doppler width in angular frequency. For the shell we may assume that $\log\alpha \sim -3$ to -4. If we use log $\alpha = -3.5$ and use an equivalent width corresponding to a velocity of $\Delta v \geq 100$ km/sec (see Figure 3) then we estimate a turbulent velocity of about 35 km/sec. If the central absorption actually consists of two components, one interstellar (expected to be strong for the observed E(B-V) = 0.16) and one stellar, then this value could easily be reduced to 20 or 25 km/sec. The small change of τ(k) for 75 and 100 km/sec also points towards a large v (turb). We adopt v (turb) = 25 km/sec with an uncertainty of about +10, −5 km/sec. The optical depth for v=0 is then increased by a factor $e^{(75/25)^2} = e^9$ as compared to the optical depth at v = 75 km/sec.

If the central absorption is not centered at 0 velocity but rather at about 10 km/sec for minimum light phases, as seems likely according to Figure 3, then the column density could be larger (the γ velocity of the star is 3 km/sec). If on the other hand v(turb) is actually larger than adopted, the optical depth is smaller.

We then find $\tau(k, 0) = 5 \cdot 10^3$ with an uncertainty of at least 2 powers of 10 because of the uncertainty in v(turb). For the column density of Mg II in the "shell" we find log N f = 16.4 ±2. With a Mg abundance of log (Mg/H) = −4.4 we derive a column density for hydrogen log N(H) = 20.8 ± 2.

If the "shell" has the average interstellar dust to gas ratio (which may not be true) and if it has the average E(B-V) per hydrogen atom then we may expect an E(B-V) = 0.1 (see Savage *et al.* 1977) from this shell with a large uncertainty. An average total color excess of E(B-V)=0.16 was observed with a possible range between 0.08 and 0.22 (Rogers and

Bell 1965). The low color excesses were found right after maximum light. Rogers and Bell apparently did not consider this variation as significant. The differences might be due to non-standard U-B and B-V colors, but it could also indicate that the dust properties in the "shell" change during the pulsational cycle, and also that only a fraction of the E(B-V) is due to true interstellar extinction.

Adopting log N(H) = 20.8 thus gives a consistent picture. Larger column densities would lead to estimates for the color excess which are inconsistent with the observations, unless the dust content in the "shell" is very low.

5. The OI lines

5.1. The line profiles

In Figure 5 we showed the line profiles of the OI emission lines. The lines are quite broad and the profiles are variable. Satellite lines seem to be present. The OI line consists of course of three components at 1302.17, 1304.87 and 1306.04 Å in the theoretical intensity ratios 2.1:1.3:0.41. In the same wavelength region we find SI lines at 1295.66, 1302.87, 1296.17, 1303.11, 1302.34 and 1305.89 Å, which are due to transitions to or from levels near the ground state.

In several spectra we see peaks around 1295, 1297 and 1289 Å of varying intensities and also of variable wavelengths. We may try to identify the peaks at 1295 and 1297 Å with the SI lines at 1295.7 and 1296.2 Å. Other SI lines would be expected at λ = 1316.6, 1323.5 and 1326.6 Å and at 1401.5, 1409.4 and 1412.9 Å but somewhat weaker than the lines around 1300 Å. These additional SI lines are never seen. Perhaps the near resonance of the SI lines around 1302 Å with the OI lines might selectively excite the levels leading preferentially to the emission at 1295.66 and 1296.17 Å, but velocity differences between OI emitting gas and the SI emitting gas of about 115 km/sec are needed to make this resonance effective.

The peak around 1289 Å might perhaps be identified with several CI lines occuring

around this wavelength. If so we should expect to see stronger CI lines around 1280 Å and 1657 Å which are not always seen when the 1289 peak is seen. CI has a near resonance level with Lyα which could perhaps lead to selective excitation in CI if velocity differences of $\sim$25 km/sec are present.

The presence of circumstellar material also opens the possibility that the satellite lines could be interpreted as being due to spatially displaced blobs of OI emission appearing in the rather large (10" $\times$ 20") entrance aperture of the IUE spectrograph which for this area acts as a slitless spectrograph. In the entrance aperture the images of these blobs are then displaced from the stellar image. If the OI emitting blobs are displaced in the direction of dispersion they appear at a wavelength different from the stellar OI line.

5.2. Spatially extended OI emission?

a. Line by line spectra

If we try to explain the apparent satellite lines of the OI line as spatially displaced OI-line- emitting blobs we must be sure that these hypothetical blobs fit within the entrance aperture. This is a necessary condition which is indeed satisfied.

Spatially extended emission can also be studied by investigating the emission along the long axis of the entrance aperture. We may see emission displaced from the stellar spectrum if the blobs are displaced in the direction perpendicular to the direction of dispersion. The IUE observatory provides spectra for different positions along the large axis of the entrance aperture, the socalled "line by line" spectra. If the spectrum is not overexposed the point spread function spreads the spectrum of a point source over 7 "lines". If the actual spectrum is spread out further it indicates spatially extended emission. The cross-sections are expected to be nearly Gaussian. In Figure 10 we show cross sections through the ℓCarinae spectra SWP 28480 and 34452 perpendicular to the direction of dispersion. (These spectra have two of the longest exposure times). One cross section refers to the wavelength band 1310 to 1410 Å, *i.e.*, outside of the OI line. "Line" 55 refers to the center of the entrance aperture. Lower

and higher "line" numbers refer to other points along the entrance aperture.

As shown by the geocoronal Lyα images of the large entrance aperture the width of the entrance aperture of 10" corresponds to about 16 Å and the edges of 20" length of the entrance aperture corresponds to "lines" 44 to 69. This means that the distance between two "lines" corresponds to about 0.8 arcsec. Spectra seen for "lines" 44 to 69 still correspond to objects seen in the large entrance aperture.

For earlier spectra half as many "lines" were extracted. The entrance aperture then extends from "line" no. 22 to 34.

b. Isophotes for the OI emission lines of ℓCarinae

Another way to check for extended OI emission is to study the isophotes for the spectra. For the "line by line" spectra we have determined a background value per pixel from the averages of "lines" 35 to 40 and subtracted this background from the flux numbers of the "line by line" spectra. Isophotes were then drawn at intervals of 1/8, 2/8, 3/8 etc. values of the maximum flux above background. Figures 11 and 12 show the isophotes around the OI line for our spectra ordered according to phase. If two spectra were taken within time intervals of a few hours we added the "line by line" spectra in order to reduce the noise. The spectrum SWP 34602, taken near maximum light phase, shows simple isophotes as expected for a stellar spectrum with a broad emission line. No indication of extended emission in the direction perpendicular to the direction of dispersion is seen. We have to remember, however, that because of the large OI fluxes at this phase the isophotes correspond to larger flux levels than for the later phases. Isophotes for lower flux levels are, however, also smooth. For later phases we see maxima in the emission fluxes for positions displaced from the stellar spectrum. We realize that an apparent peak seen in the line profiles (Figure 11) around the wavelength of 1280 Å is often due to these displaced emission maxima.

It is interesting to follow the apparent motion of the emission blobs during advancing phases. For phase 0.099 *i.e.*, SWP 34602, we see rather smooth isophotes. The extent

in the direction of dispersion is, however, quite broad, extending over 15 Å. This either shows improbably high velocities or, more likely, contributions from several lines as discussed previously.

At phase 0.183, 3 days later, we see some irregularities develop in the isophotes. Spatially extended emission seems to be indicated at several points. The 1293 Å peak appears to become relatively stronger, which could also mean that a spatially displaced OI emitting blob may appear at this wavelength. The central peak of the OI line has shifted by about 3 Å to shorter wavelengths. The spectra of the next phases shown were actually taken during the previous period and may therefore be related to the earlier phases only if the phenomenon is a periodic one. For phases around 0.587 new blobs have developed and for phases around 0.72 again a new intense blob appears. While this is strongest on the spectrum SWP 34460 it is already visible in SWP 34458 and is still recognizable in the SWP 34462 spectrum as seen in Figure 13. We therefore believe that it is real and not a hit. Five periods later at phase 0.4 the isophotes look very broad and rugged but not spatially extended along the long axis of the entrance aperture.

It is surprising that position changes for emission blobs can be seen for time intervals of only 2 hours. ℓCarinae is at a distance of about 400 pc. The blobs appear to change their position by several arcsec, which means by a distance of more than 1000 a.u. or more than $1.5 \cdot 10^{16}$ cm. To travel this distance in 2 hours velocities larger than the velocity of light would be required. The only explanation for such apparent position changes is the "lighthouse" effect. The gas excited at slightly different times must be at slightly different distances from the exciting source, or at slightly different distances from us.

If we assume that the light pulse is associated with the phase of maximum light and the spatially displaced emission occurs about 5 days later we find that the light can travel $1.5\ 10^{16}$ cm or 1000 a.u. during that time, corresponding to 2.5 arcsec for the distance of ℓCarinae, a distance which is in rather good agreement with the observed displacements of

the first emerging blobs at phase 0.18.

We find it, however, very surprising that the emission of some blobs can decay so fast. The exciting light pulse must be very short lived and the excited gas blob must be of very small extent (only a few a.u.) such that the emission can decay during a few hours. If the OI emission is due to the resonance with Ly β it must mean that Ly β is absorbed over a distance of a few a.u. or that the velocity differences make the resonance disappear.

The question remains whether this extended emission was a special event which happened to occur during our time of observation, perhaps due to a large flare, or whether it is a periodic phenomenon. The slightly extended emission at phase 0.183, one period later than most of the other spectra, seems to tell us that there is periodicity in the event. On the other hand the exposure SWP 36181 taken 5 periods later does not fit into the sequence of the other spectra.

The "shell" seen in the Mg II is expected to cause absorption also in the OI lines. We expect a column density of about log N(O)=17.8 $\pm$ 2 for solar abundances. We do not see strong absorption in the OI lines, but because of the low resolution (4 Å at 1300 Å) any absorption within an interval of 100 km/sec (as seen in the Mg II lines), if occuring in several lines mixed with the emission in those lines, will be difficult to recognize. High resolution spectra would be needed for a proper study of the OI line emission as a function of phase.

In Figure 14 we have plotted the intensity weighted average velocity of the broad O I feature as a function of phase. Systematic shifts by up to 5 Å are seen. The longest wavelengths are found for maximum light, the shortest ones for the phases after the strong blobs occurred. We suspect that the large wavelength measured during maximum light phases may be due to absorption in the strongest O I line around 1302 Å, making the 1304 line more prominent. The shifts to shorter wavelengths during minimum light phases are probably caused by relatively stronger emission around 1295 Å.

If extended emission is seen in the OI lines we may wonder whether such an extended

emission can also be seen in the Mg II lines. For this purpose we have studied the low resolution (long wavelengths *i.e.*, 2000 Å $< \lambda <$ 3000 Å) spectra of ℓCarinae. The contour diagrams for the Mg II lines do not show recognizable spatial extend. Only for the lowest flux levels above background may we see a suggestion of a possible asymmetry in the isophotes. This may, however, well be noise.

We suspect that the extended emission is only visible in OI because of the resonance with Lyβ. It might then possibly be visible also in Hα.

6. The Continuum

6.1. The flux around 1950 Å

In Figure 15 we have plotted the continuum flux at 1950 Å, *i.e.*, the fluxes seen in between the strong absorption lines over an interval of about 50 Å. These are probably not the correct "continuum" fluxes because for this low resolution several weaker absorption lines still reduce the measured fluxes. For a relative comparison these "continuum" fluxes are, however, still useful. We did not correct for interstellar absorption, which gives a constant factor for all 1950 Å fluxes, and we did not correct for the degradiation of the camera sensitivity, because the uncertainties in the measurement are larger than the 10% changes in the camera sensitivity. The point at phase 0.912 may have to be raised by about 10% relative to the measurements of 1980 because of the changing sensitivity of the camera. Data measured for phases around 0.05 do, however, not indicate the necessity for such a correction.

The UV fluxes show the temperature maximum to occur at phase 0.95 $\pm$ 0.02, in agreement with results obtained from the B-V colors. This also appears to be the phase at which the CIV lines have their largest flux. The 1950 Å fluxes may perhaps show a slight increase for phases between 0.65 and 0.8, possibly due to a buildup of a low temperature chromosphere. But this needs confirmation.

6.2. The flux around 1500 Å

As seen in Figure 1 there is a non zero flux around 1500 Å at all phases. This is surprising for a star with such low T_{eff}. It is often assumed that for the cool giants and supergiants the flux seen at these wavelengths is due to longer wavelength light scattered in the IUE spectrograph.

In Figure 15 we have also plotted the phase dependence of the flux around 1500 Å. If it is scattered light from somewhat longer wavelengths it would be expected to follow the 1950 Å curve or perhaps the visual light curve because this star is so bright in the optical region. Between phases 0.7 and 1 the optical light changes by a factor of 2.2. The flux at 1950 Å increases by a factor of 25. The flux at 1500 Å changes by a factor of about 16, not very different from the factor observed for the 1950 Å flux. In detail the phase dependence of these two fluxes is, however, very different. The 1950 Å flux peaks at phase 0.95 while the 1500 Å flux peaks at phase 1. At phase 1.1 the 1950 Å flux has decreased by a factor of 10 while the 1500 Å flux has changed only by a factor of 2.7. There must be intrinsic emission at 1500 Å. At both wavelengths the flux appears to be somewhat enhanced at phases between 0.7 and 0.8. The flux at 1500 Å shows a weak secondary maximum for phases between 0.4 and 0.6 when the visual and the 1950 Å curves both have a minimum. The wavelength dependences for several of the 1500 Å humps are shown in Figure 16.

Figure 17 shows the wavelength dependence of the dark sky spectrum studied by Crenshaw, Bruegman and Norman (1990). These authors call the dark sky spectrum the "artifact" spectrum, implying that it is not real but due to the IUE reduction procedure for very weak sources. In a qualitative way there is some similarity between this socalled "artifact" spectrum and the energy distribution observed by us for ℓCarinae in the 1500 Å region, but the fluxes observed for ℓCarinae in the SWP 34465 and 34458 spectra are about $8 \cdot 10^{-15}$ while they are about $1.5 \cdot 10^{-15}$ in the dark sky spectrum. This means for ℓCarinae they are about a factor 5 larger than for the dark sky. Since the emission seen in the ℓCarinae spectra is much larger than the one seen in the dark sky, and since

the phase dependence of the 1500 Å flux is different from the one observed for the longer wavelengths, we conclude that the emission seen is intrinsic to ℓCarinae. Considering the noise the wavelength dependence of the 1500 Å bump in the dark sky spectrum is not very different from the bump seen in the ℓCarinae spectrum. This raise the possibility that the emission hump seen in the dark sky spectrum around 1500 Å may be real too, possibly due to the same kind of particles which cause the emission in ℓCarinae. Clearly more studies are needed to clarify this point.

7. Conclusions

We observed the emission lines of the long period Cepheid ℓCarinae as a function of phase. Our primary aim was to see whether CII or CIV emission occurs earlier in the cycle in order to see whether a transition layer or a shockwave is responsible for the emission. Unfortunately observations for phases between 0.8 and 0.9 are missing. These turned out to be very important in order to observe the onset of the CIV emission. From the available data it appears, however, that the CIV emission may occur first. During phases when both lines are measurable the ratio of the CIV to CII line fluxes is much larger than seen in solar type transition regions, making it very unlikely that we see transition layer emission. It then seems that even for ℓCarinae, which is right at the red edge of the Cepheid instability strip, convection is either not strong enough or does not persist long enough for a transition layer to develop. In the Mg II line we may possibly see the formation of a chromosphere, but we cannot be sure.

Rogers and Bell (1965) suspected circumstellar gas because of an Hα absorption component, which does not change during the pulsational cycle. We also see strong central absorption over a wide velocity range ($> \pm$ 75 km/sec) in the Mg II lines, which we attribute to circumstellar gas. Such large velocity range can hardly be expected for interstellar gas. We think we also see emission of this circumstellar gas in our spectra in OI line blobs observed out to several arcseconds away from the star. It would be very interesting to take an image

with high spatial resolution in a wavelength band including the OI emission line.

The circumstellar column density of this gas is probably of the order of 10^{21} hydrogen atoms per cm^2.

The strength of the OI line, if excited by Lyβ, suggests strong Lyβ emission at least during part of the cycle. We may therefore also expect to see extended weak emission in Hα.

Using a column density of 10^{21} atoms/cm^2 for the cloud in front of ℓCarinae and using a radius r of 1000 AU, as suggested by the OI blobs, we find for the mass of the cloud $M \sim 10^{-3}$ $M_\odot$ and a density of 7×10^4 particles per cm^3 (assuming a homogeneous sphere). If we assume an expansion velocity of about 35 km/sec, comparable to the estimated turbulence velocity (and perhaps suggested by the two dips in the central absorption), then we find a mass loss of about $M = 2 \times 10^{-5}$ $M_\odot$/year with an estimated uncertainty of at least 2 powers of 10.

We can compare these estimates with those obtained for other Cepheids. McAlary and Welch (1986) find from the infrared excess for the "cloud" around R TrA (with a period of 3.4 days) a radius between 10^{15} to 10^{16} cm, *i.e.*, the same order of magnitude which we estimate here for the ℓ Carinae cloud. The inferred mass loss for R TrA is, however, only a few times 10^{-9} $M_\odot$ per year. RS Pup with a period of 41 days has been found to have nebulosity around it (Havlen 1972). It has a large infrared excess (Deasy and Butler 1986), from which McAlary and Welch determine a mass of 0.03 $M_\odot$. The radius is nearly 1 pc. That nebula is apparently much larger and more massive than estimate of here for ℓ Carinae. Deasy (1988) estimates a mass loss of $M = 3.5 \times 10^{-6}$ $M_\odot$ for RS Pup with an upper limit of 10^{-5} $M_\odot$ per year. This is not very different from our rough estimate for ℓ Carinae, but ℓ Carinae has no detectable infrared excess.

It is interesting to note that for the Cepheid binary S Muscae with a pulsation period of 9.6 days we could put a low upper limit to the mass loss, namely $dM/dt < 10^{-9}$ $M_\odot$ per year (Rodrigues and Böhm-Vitense 1992). For ℓ Carinae with a period of 35.5 days we have

presented here indirect evidence for a strong mass loss in rough agreement and probably not in excess of values that Reimers found for other cool, luminous supergiants. This trend is similar to the finding by Deasy and Butler (1986) that short period Cepheids (period < 15 days) do not show infrared emission larger than non-variable supergiants. For these they find mass loss rates of 10^{-7} to 10^{-8} $M_{\odot}$ per year. R TrA wit a period of 3.4 days was found by McAlary and Welch to have a small mass loss while RS Puppis with a long period has a strong mass loss. It will be interesting to find out more about the dependence of mass loss on the pulsation period.

A continuous emission around 1500 Å is observed whose origin is at present unknown. This emission is possibly also seen in the dark sky.

Table 1a

Data for low resolution short wavelength IUE spectra

Image no	Observ. date			log FES	JD	Expos.	Puls.	Roll angle	
SWP	Year	Day	UT	counts	2440000+	time[m]	phase	[°]	Observer
10477	1980	300	03:28	3.004	4538.644	20	0.941	287	Schmidt
10486	1980	301	09:25	2.998	4539.892	20	0.976	286	Schmidt
10490	1980	302	05:10	3.050	4540.715	60	0.999	285	Schmidt
10492	1980	302	13:22	3.017	4541.057	50	0.009	285	Schmidt
10502	1980	304	00:10	2.950	4542.447	110	0.049	283	Schmidt
10513	1980	305	08:19	2.968	4543.847	60	0.088	282	Schmidt
10515	1980	305	12:40	2.968	4544.028	53	0.093	282	Schmidt
26973	1985	297	16:08	2.833	6363.172	25	0.255	290	Deasy
28418	1986	153	10:07	2.715	6583.922	315	0.462	68	Willson
28480	1986	164	08:10	2.697	6594.840	270	0.769	58	Willson
33669	1988	150	14:37	2.920	7311.109	30	0.912	71	B.-V.
34429	1988	281	06:30	2.654	7441.771	60	0.586	308	B.-V.
34430	1988	281	08:43	2.653	7441.863	70	0.588	308	B.-V.
34444	1988	283	10:43	2.654	7443.947	60	0.647	306	B.-V.
34445	1988	283	12:31	2.670	7444.021	35	0.649	306	B.-V.
34451	1988	285	07:01	2.657	7445.792	97	0.699	304	B.-V.
34452	1988	285	11:34	2.643	7445.982	150	0.704	303	B.-V.
34458	1988	285	23:49	2.663	7446.492	180	0.719	303	B.-V.
34460	1988	286	06:59	2.663	7446.791	150	0.727	302	B.-V.
34462	1988	286	11:51	2.656	7446.994	118	0.733	302	B.-V.
34464	1988	286	23:59	2.672	7447.500	180	0.747	302	B.-V.
34465	1988	287	11:25	2.672	7447.976	170	0.760	301	B.-V.
34470	1988	288	03:27	2.699	7448.644	168	0.779	301	B.-V.
34557	1988	297	12:06	2.907	7458.004	84	0.043	290	B.-V.

34602	1988	299	12:15	2.875	7460.010	68	0.099	288	B.-V.
34617	1988	302	12:21	2.821	7463.015	55	0.183	285	B.-V.
36181	1989	122	18:00	2.699	7649.250	100	0.420	97	B.-V.
39117	1990	171	14:12	2.912	8063.092	160	0.058	51	Teays
39179	1990	186	07:32	2.718	8077.814	390	0.475	39	Teays

Table 1b

IUE long wavelength, high resolution spectra of ℓCarinae

Image no	Observ. date			log FES	JD	Expos.	Puls.	
LWR	Year	Day	UT	counts	2440000+	time[m]	phase	Observer
6654	1980	013	22:37	2.950	4252.442	32	0.892	Schmidt
9146	1980	300	02:56	3.003	4538.622	35	0.941	Schmidt
9158	1980	301	08:55	3.009	4539.871	25	0.976	Schmidt
9168	1980	302	04:22	3.005	4540.682	27	0.998	Schmidt
9186	1980	303	22:53	2.989	4542.453	30	0.049	Schmidt
9203	1980	305	13:00	2.972	4544.044	32	0.093	Schmidt
LWP								
3208	1984	114	03:55	2.771	5813.663	45	0.801	Deasy
3209	1984	114	08:18	2.757	5813.846	58	0.806	Deasy
6985	1985	297	16:59	2.834	6363.208	60	0.255	Deasy
7049	1985	310	05:10	2.687	6375.715	55	0.607	Mullan
8034	1986	105	18:52	2.881	6536.286	50	0.123	Mullan
14186	1988	281	07:33	2.651	7441.815	50	0.587	B.-V.
14193	1988	283	11:41	2.656	7443.987	45	0.648	B.-V.
14207	1988	285	08:22	2.658	7445.848	50	0.700	B.-V.
14212	1988	286	01:51	2.661	7446.577	50	0.721	B.-V.
14215	1988	287	02:03	2.690	7447.585	50	0.749	B.-V.

Table 1c

IUE low resolution long wavelength spectra of ℓCarinae

Image no	Observ. date			log FES	JD	Expos.	Puls.	
LWR	Year	Day	UT	counts	2440000+	time[m]	phase	Observer
5509	1979	247	11:36	2.947	4120.976	2.0	0.194	Schmidt
9147	1980	300	03:54	3.004	4538.662	15.0	0.942	Schmidt
9159	1980	301	09:53	3.008	4539.911	14.0	0.977	Schmidt
9169	1980	302	06.00	3.022	4540.750	12.0	0.001	Schmidt
LWP								
8380	1986	164	05:47	2.691	6594.740	1.0	0.769	Willson
14192	1988	283	10:02	2.645	7443.918	6.0	0.646	B.-V.
14206	1988	285	06:01	2.644	7445.750	5.0	0.698	B.-V.
14211	1988	285	22:08	2.682	7446.422	5.0	0.717	B.-V.
14214	1988	286	22:19	2.678	7447.430	5.0	0.745	B.-V.
18150	1990	171	12:46	2.912	8063.032	0.3	0.055	Teays
18151	1990	171	15:37	2.912	8063.151	0.5	0.060	Teays
18290	1990	186	04:09	2.718	8077.673	1.5	0.470	Teays

Table 2

Emission line fluxes in ergs cm^{-2} sec^{-1}

SWP	Phase	f (OI) $\times 10^{14}$	λ[A] OI	f (CII) $\times 10^{14}$	λ[A] CII	f (CIV) $\times 10^{14}$	λ[A] CIV
10477	0.941	73.2	1303.1789	<10	1336.533	103	1549.357
10486	0.976	128	1304.541	18.9	1334.116	92	1547.954
10490	0.999	230	1302.349	<6.4	1335.260	26	1549.813
10492	0.009	209	1302.141	10.7:	1330.882	21	1547.760
10502	0.049	248	1303.269	3.6	1335.484	<11	1544.811
10513	0.088	241	1301.652	4.1:	1330.908	<1	···
10515	0.093	238	1302.522	4.9	1333.492	···	···
26973	0.255	111	1300.243	···	···	···	···
28418	0.462	12.3	1299.725	<1.8	1331.954	<1	1551.984
28480	0.769	36.8	1300.640	2.2:	1336.780	···	···
33669	0.912	100.0	1301.969	<3.0	···	12:	1547.701
34429	0.586	43.8	1300.094	1.9:	1337.132	≤1	1552.620
34430	0.588	69.0	1298.884	13.0:	1339.250	≤4	1546.922
34444	0.647	42.7	1299.621	···	···	≤8	1552.149
34445	0.649	32.8	1300.694	5.0:	1338.226	···	···
34451	0.699	30.0	1299.709	···	···	≤2	1547.657
34452	0.704	>26.0	1302.442	···	···	≤4	1550.599
34458	0.729	28.6	1300.700	<1.6	1336.286	≤2	1551.990
34460	0.727	46.2	1298.888	<1.	1328.775	···	···
34462	0.733	40.3	1298.668	3.3:	1334.399	≤2	1551.240
34464	0.747	34.2	1298.874	<0.9	1329.258	≤6	1550.680
34465	0.760	36.4	1299.811	4.1:	1334.005	≤1	1550.550
34470	0.779	38.1	1300.343	<3.3	1337.180	≤3	1549.544
34557	0.043	254	1301.280	<7.0	···	≤4	1548.021
34602	0.099	218	1301.510	14.	1338.240	≤3	1551.854
34617	0.183	172	1300.386	···	···	≤2	1553.330

36181	0.420	64.8	1300.870	<7.	1339.041	15:	1552.576
39117	0.058	227	1302.017	3.4:	1336.481	3:	1553.020
39179	0.475	59.9	1301.257	4.6:	1338.810	...	...

Table 3

Peak fluxes for the MgII lines in units of 10^{-12} ergs cm^{-2} sec^{-1} $Å^{-1}$

for the "blue" and "red" wings of the k and h lines

Phase	$f(k_b)$	$f(k_r)$	$f(h_b)$	$f(h_r)$	$f(k_b)/f(h_b)$
0.700	2.2	3.0	2.6	2.7	0.85
0.721	2.8	3.2	3.7	3.2	0.74
0.749	3.2	3.8	4.4	3.8	0.72
0.801	3.9	3.9	5.1	4.0	0.67
0.806	4.3	4.3	5.1	3.7	0.84
0.892	6.2	4.3	6.8	4.0	0.91
0.941	14.1	7.1	14.8	6.7	0.95
0.976	13.9	8.4	12.9	7.3	1.08
0.998	13.3	9.0	10.7	7.6	1.24
0.049	10.3	8.7	7.8	7.2	1.32
0.093	8.4	7.9	6.6	6.4	1.27
0.123	6.4	6.5	5.0	5.8	1.28
0.255	2.8	4.5	2.2	2.9	1.25
0.587	1.0:	2.3	1.25	1.8	0.80
0.648	1.6	2.4	2.0	2.4	0.80

References

Bernat, A. P. and Lambert, D. L. 1976, ApJ, 204, 830

Böhm-Vitense, E., Garnavich, P., Lawler, M., Mena-Werth, J., Morgan, S., Peterson, E. and Temple, S. 1989, ApJ, 343, 343

Böhm-Vitense, E. and Querci, M. 1988, In "Exploring the Universe with the IUE Satellite", ed. Y. Kondo, Reidel Dordrecht, p. 223

Crenshaw, D. M., Bruegman, O. W. and Norman, D. J. 1990, PASP, 102, 463

Dalgarno, A., Herzberg, G. and Stephens, T. L. 1970, ApJ, 162, L49

Deasy, H. P. 1988, MNRAS, 231, 673

Deasy, H. P. and Butler, C. J. 1986, Nature, 320, 726

Havlen, R. J. 1972, A&A, 16, 252

McAlary, C. W. and Welch, D. L. 1986, AJ, 91, 1209

Rodrigues, L. and Böhm-Vitense, E. 1992, ApJ submitted

Rogers, A. W. and Bell, R. A. 1968, MNRAS, 138, 23

Savage, B. D., Bohlin, R. C., Drake, J. F. and Budich, W. 1977, ApJ, 216, 291

Schmidt, E. G. and Parsons, S. B. 1982, ApJ, 279, 202 and 215

Schmidt, E. G. and Parsons, S. B. 1982, ApJS, 48, 185

Stibbs, D. W. N., 1955, MNRAS, 138, 23

Unsöld, A. 1955, In "Physik d. Sternatmosphären", Springer Verlag, Berlin, Heidelberg, p. 265.

Figure Captions

Figure 1a. The FES counts, measuring the brightness of the star during the observations are plotted as a function of phase. In Figure 1b we have plotted the radial velocities as a function of phase according to Stibbs 1955.

Figure 2. Low resolution, short wavelength spectra of ℓCarinae are shown for different phases P.

Figure 3. The line profiles of the MgII lines are shown as a function of velocity, calculated from the wavelength differences from the line centers, which are adopted to be at the wavelengths given in the plots. The phases P and the IUE catalog numbers of the spectra are also given.

Figure 4. The CIV (dots) and OI (diamonds) line fluxes are shown as a function of phase P.

Figure 5. The OI line profiles are shown as a function of wavelength for different phases P. The IUE catalogue numbers of the spectra are also given.

Figure 6. For the MgII k lines at 2795.528 Å the peak fluxes for the "red" and "blue" wings are shown as a function of pulsational phase P.

Figure 7. For the MgII h line at 2802.704 Å the peak fluxes for the "red" and "blue" wings are shown as a function of pulsational phase P.

Figure 8. For the "blue" wing the peak fluxes in the h and k lines are plotted as a function of phase. They refer to velocities of about -75 km/sec.

Figure 9. For the "red" wings the peak fluxes in the h and k lines are plotted as a function of phase. During minimum light phases they refer to velocities around 75 km/sec., during maximum light they refer to velocities around $\sim$ 100 km/sec.

Figure 10. Cross-sections perpendicular through the spectra SWP 28480 and SWP 34452 are shown. They are assymetric with respect to the center of the spectrum. Figure a refers to a wavelength band 1310 to 1410 Å, Figure 2 to 1298-1305 Å.

Figure 11. OI contour diagrams for the spectra taken by us are shown for different phases. For spectra taken at intervals af a few hours or less two spectra were added in order to reduce the noise. Only contour lines for fluxes above the average flux are shown. For low flux levels extended emission in different directions is seen.

Figure 12. OI contour diagrams are shown for spectra taken by other observers are shown in succession of phase. These diagrams refer to much earlier or much later cycles than the diagrams in Figure 10. Note that for SWP 39117 the vertical scale is different.

Figure 13. The isophotes for the SWP spectra SWP 34458, 34460 and 34462 are shown. The strong emission blob in SWP 34460 is seen already in SWP 34458 and still recognizable in SWP 34462 though at low flux levels.

Figure 14. The intensity weighted average wavelength of the head O I feature is plotted as a function of phase. The x refer to our own observations, the encircled symbols to spectra taken by other observers. For some low values the corresponding SWP numbers have been noted.

Figure 15. The top graph shows the continuum fluxes around 1950 Å as a function of phase. The diamonds refer to our measurements the encircled symbols to spectra taken by other observers. The triangles give the measured C IV line fluxes (scale on the right). The bottom graph shows the continuum fluxes around 1500 Å as a function of phase. A secondary maximum is measured for phases around 0.55.

Figure 16. The energy distribution around 1500 Å is shown for several spectra of ℓCarinae.

Figure 17. The energy distribution of the dark sky is shown as derived by Crenshaw, Bruegman and Norman (1990).

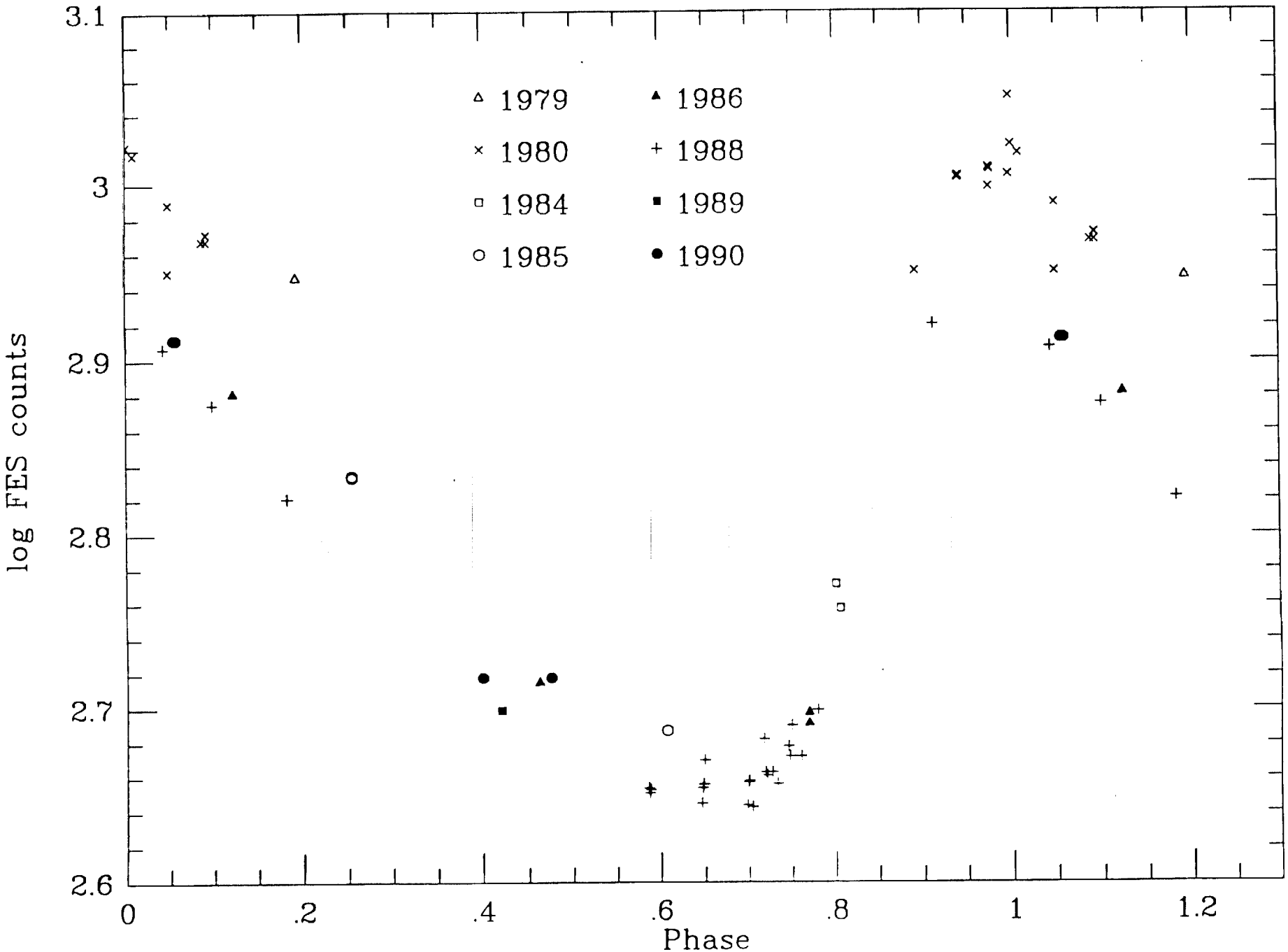
3.1
3
2.9
2.8
2.7
2.6
log FES counts
0
.2
.4
.6
.8
1
1.2
Phase
1979
1980
1984
1985
1986
1988
1989
1990

Figure 1a

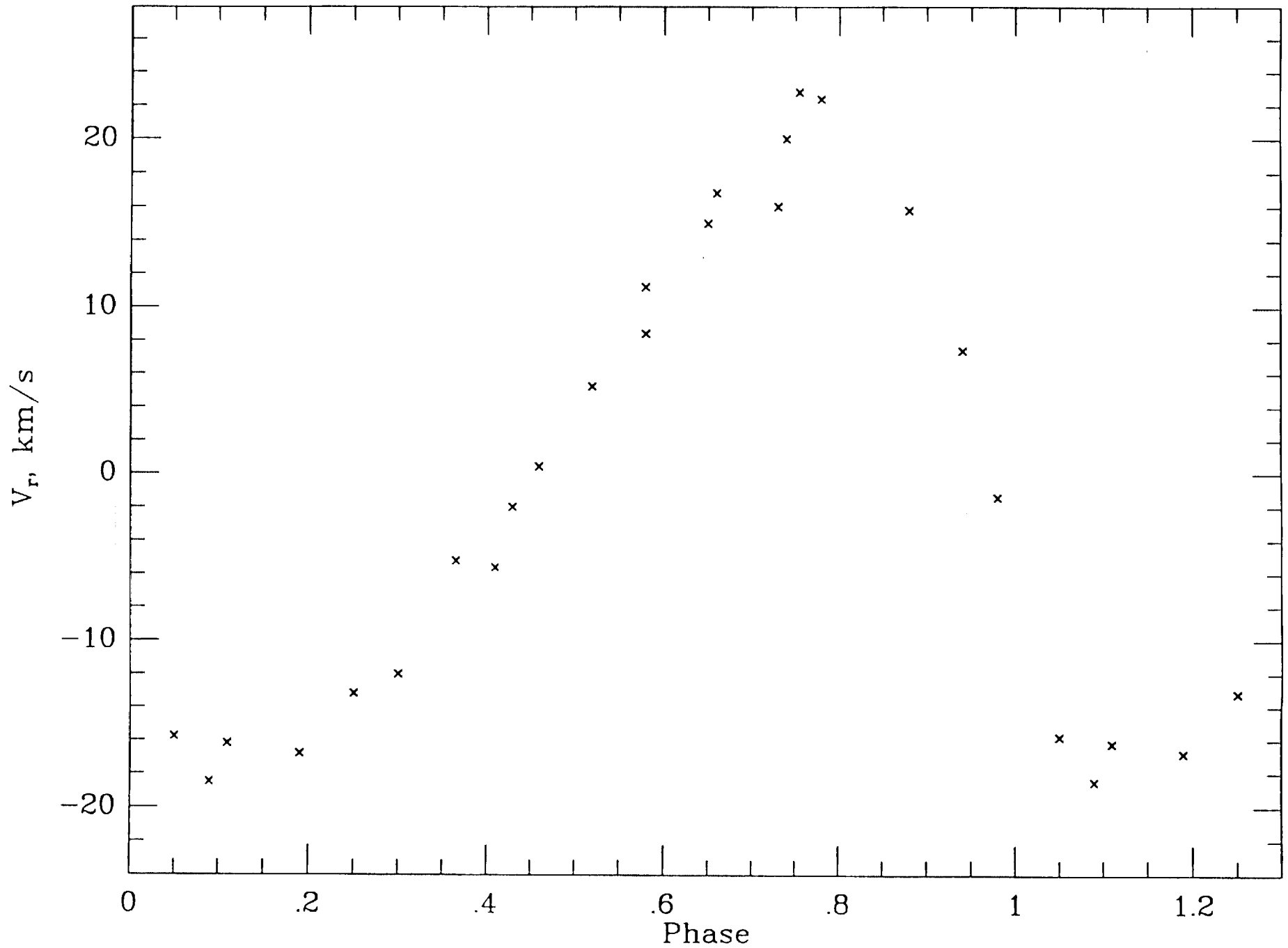

Figure 16

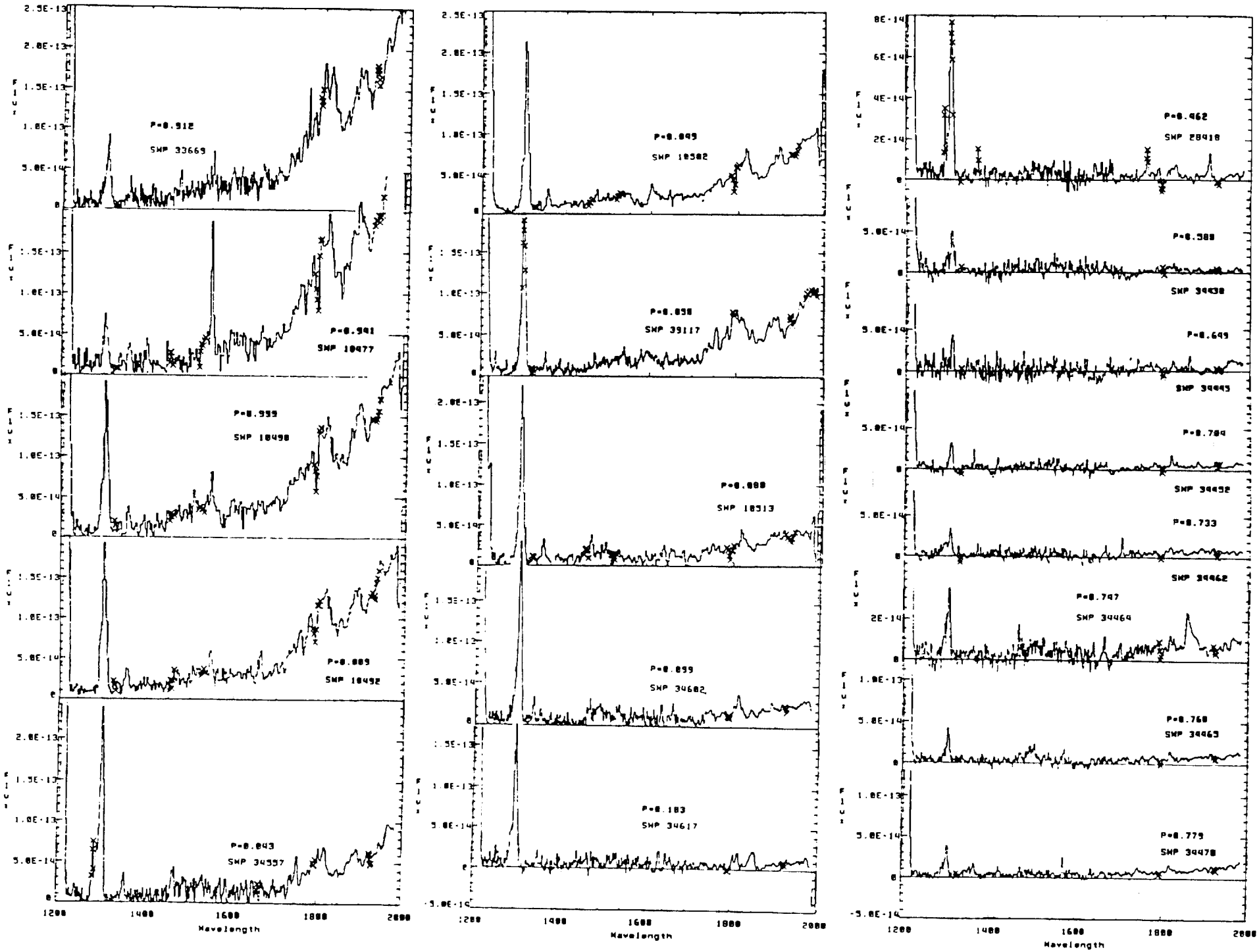
P=0.912
SWP 33669
P=0.981
SWP 18477
P=0.955
SWP 18498
P=0.889
SWP 18492
P=0.843
SWP 34597
P=0.849
SWP 18582
P=0.838
SWP 35117
P=0.888
SWP 18513
P=0.899
SWP 34682
P=0.183
SWP 34617
P=0.462
SWP 28918
P=0.588
SWP 34438
P=0.649
SWP 34443
P=0.784
SWP 34452
P=0.733
SWP 34462
P=0.747
SWP 34464
P=0.768
SWP 34463
P=0.779
SWP 34478
Wavelength

Figure 2

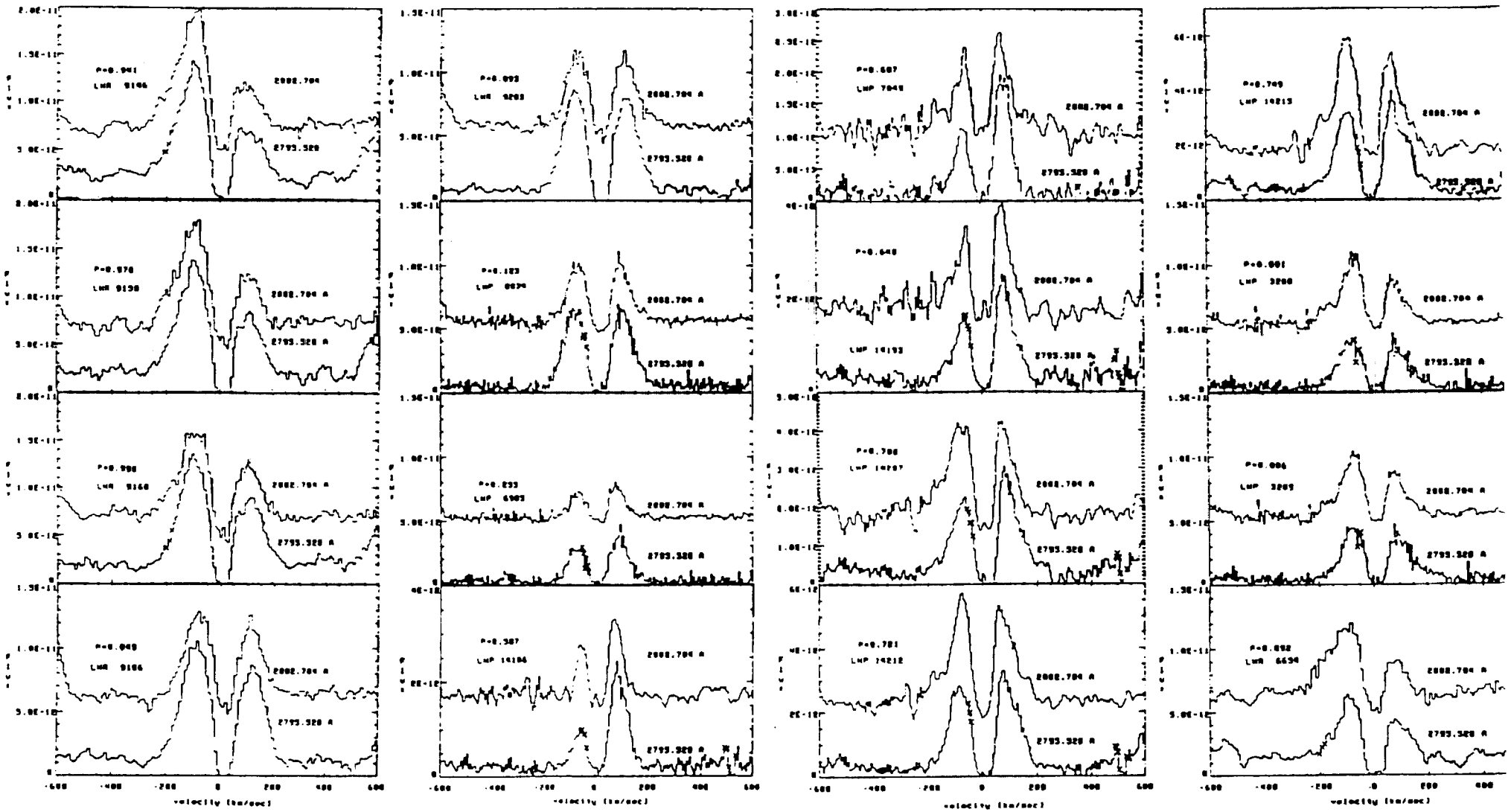

Figure 3

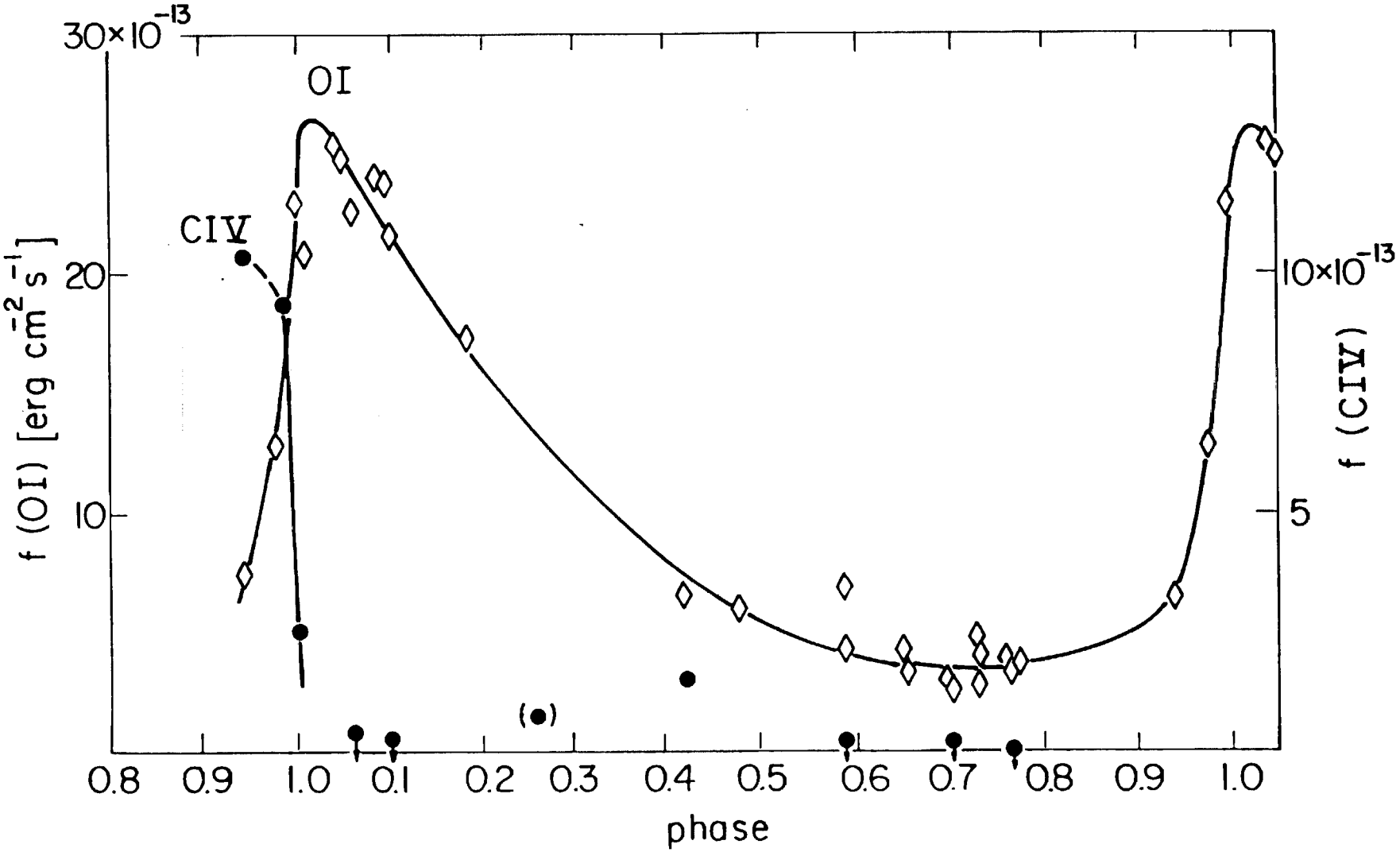

Böhm-Vitense + Love

Figure 4

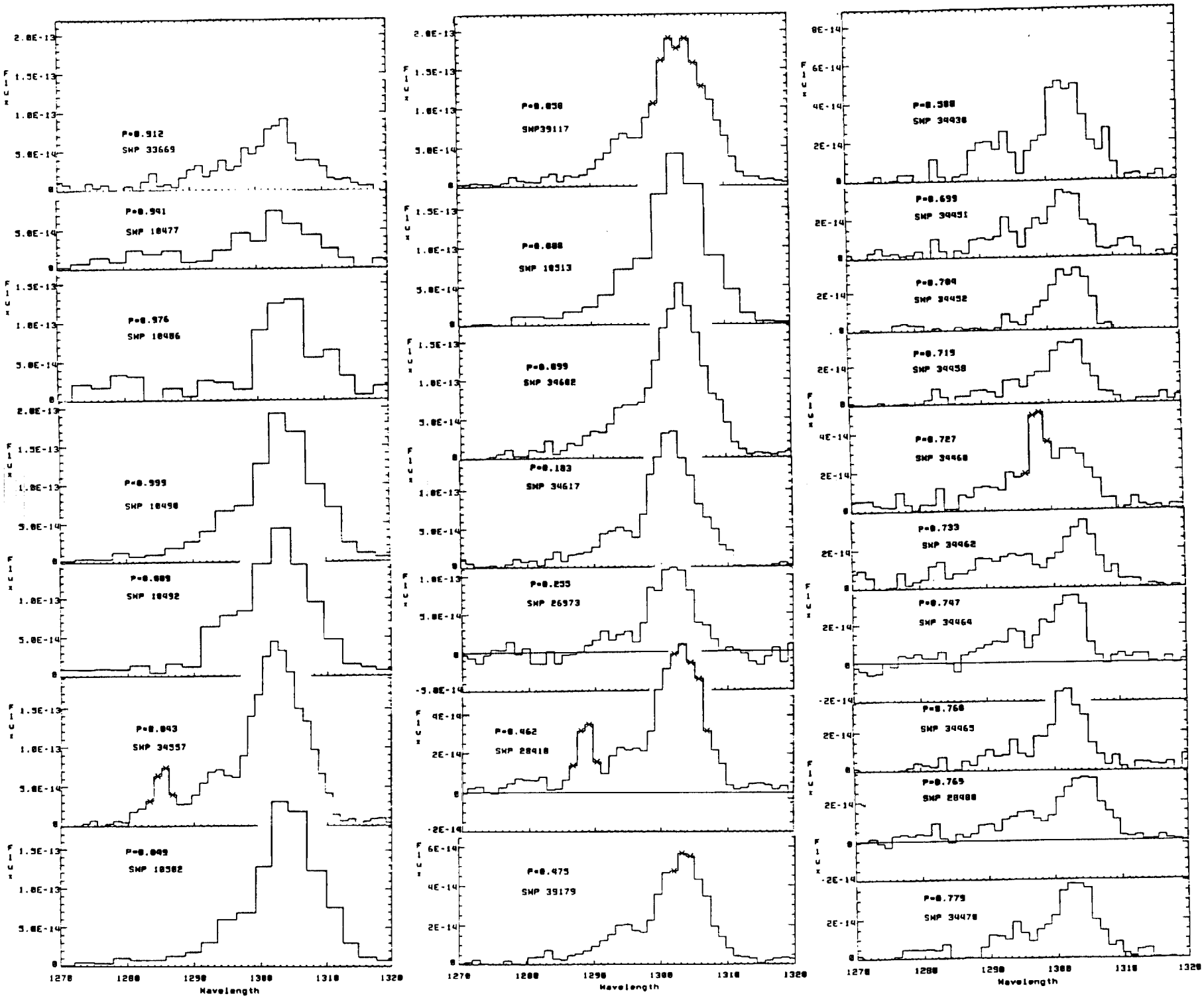
P=0.912
SWP 33669
P=0.941
SWP 18477
P=0.976
SWP 18486
P=0.999
SWP 18498
P=0.009
SWP 18492
P=0.043
SWP 34557
P=0.049
SWP 18502
P=0.838
SWP39117
P=0.888
SWP 18513
P=0.899
SWP 34682
P=0.183
SWP 34617
P=0.255
SWP 26973
P=0.462
SWP 28418
P=0.475
SWP 39179
P=0.588
SWP 34436
P=0.699
SWP 34451
P=0.709
SWP 34452
P=0.719
SWP 34458
P=0.727
SWP 34468
P=0.733
SWP 34462
P=0.747
SWP 34464
P=0.760
SWP 34465
P=0.769
SWP 28488
P=0.779
SWP 34478
1278
1288
1298
1308
1318
1328
Wavelength

Fig 5

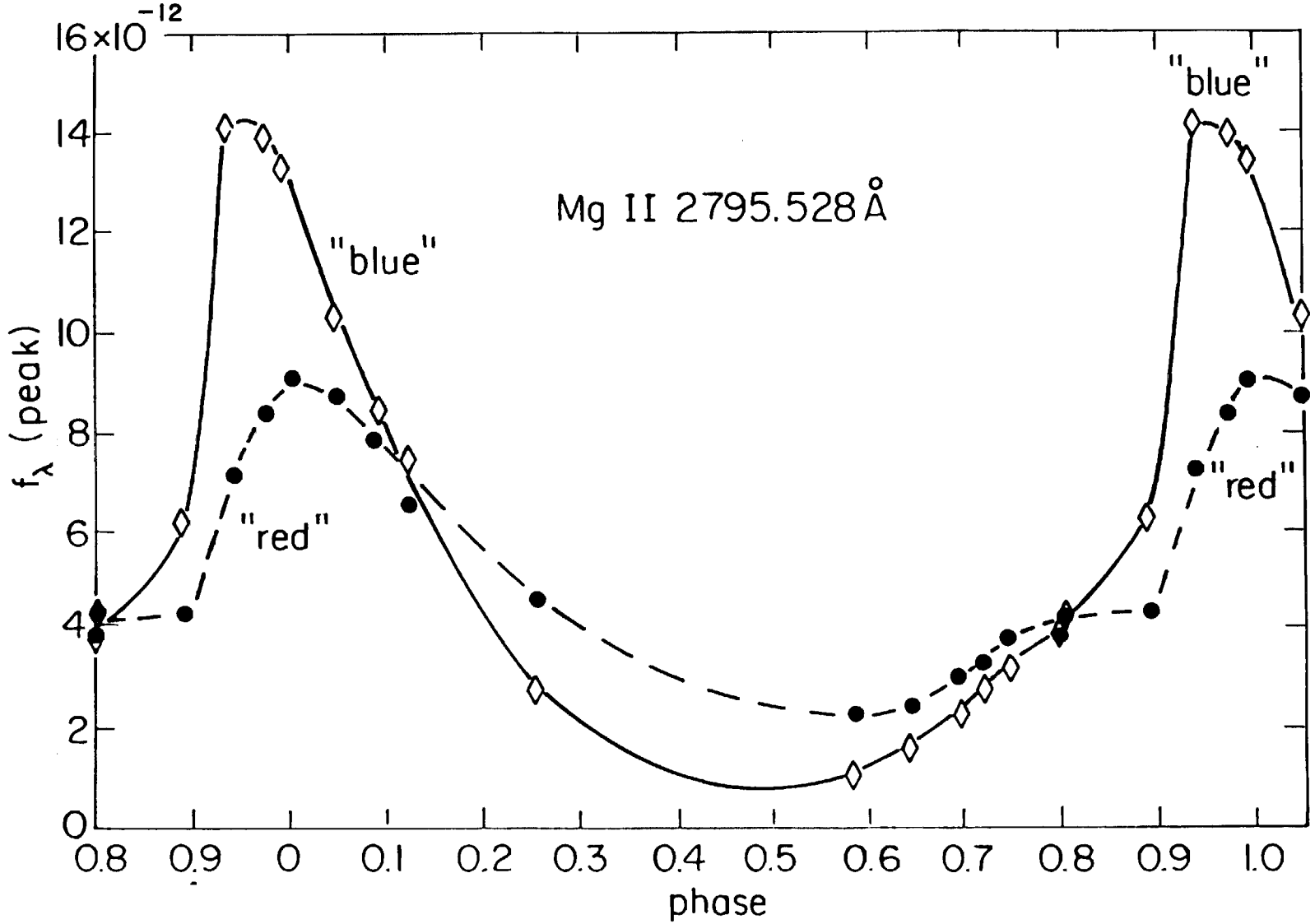
16×10⁻¹²
14
12
10
8
6
4
2
0
f_λ (peak)
Mg II 2795.528 Å
"blue"
"red"
"blue"
"red"
0.8
0.9
0
0.1
0.2
0.3
0.4
0.5
0.6
0.7
0.8
0.9
1.0
phase

Fig 6

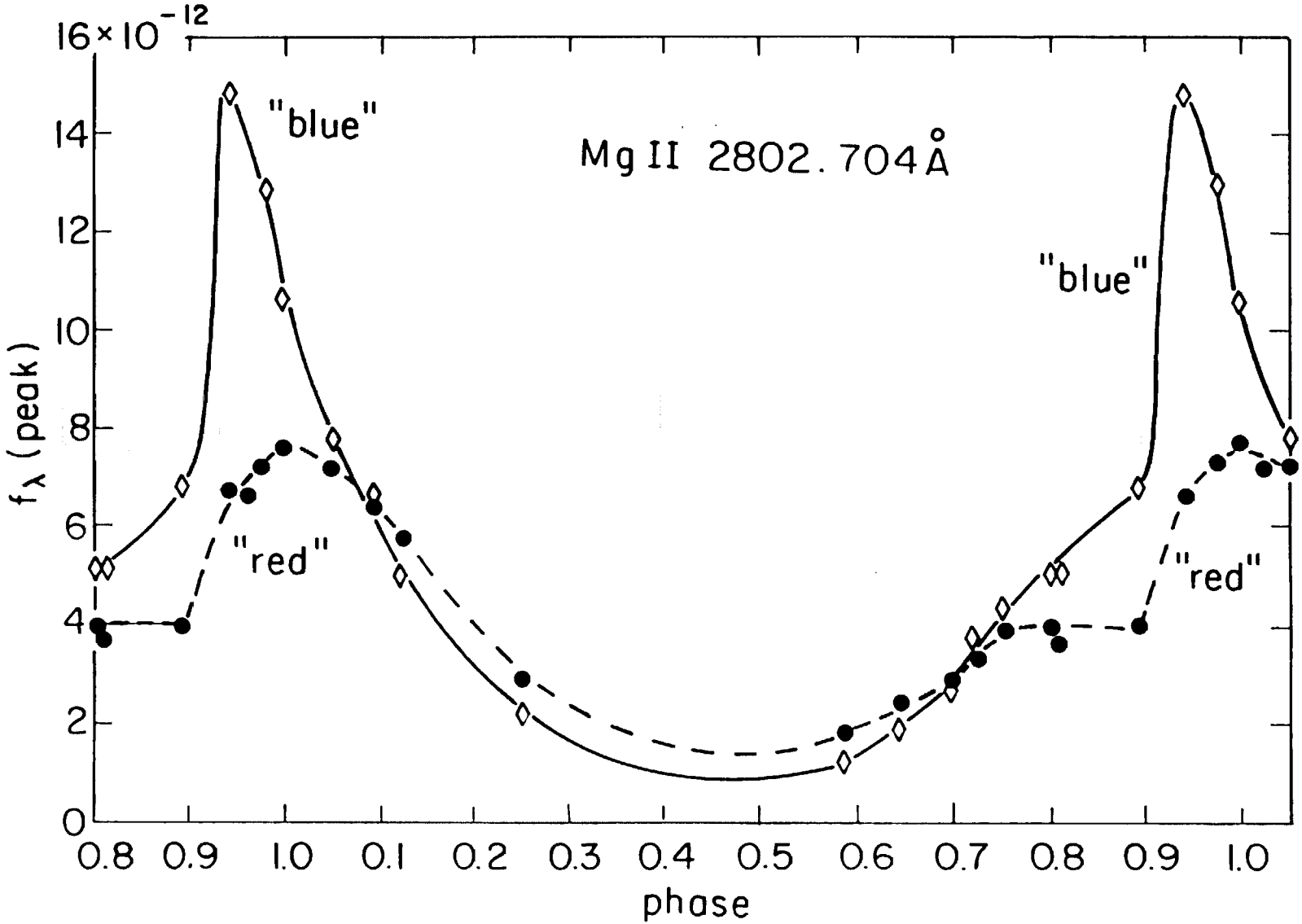
16×10⁻¹²
14
12
10
8
6
4
2
0
f_λ (peak)
"blue"
Mg II 2802.704 Å
"blue"
"red"
"red"
0.8 0.9 1.0 0.1 0.2 0.3 0.4 0.5 0.6 0.7 0.8 0.9 1.0
phase

Figure 9

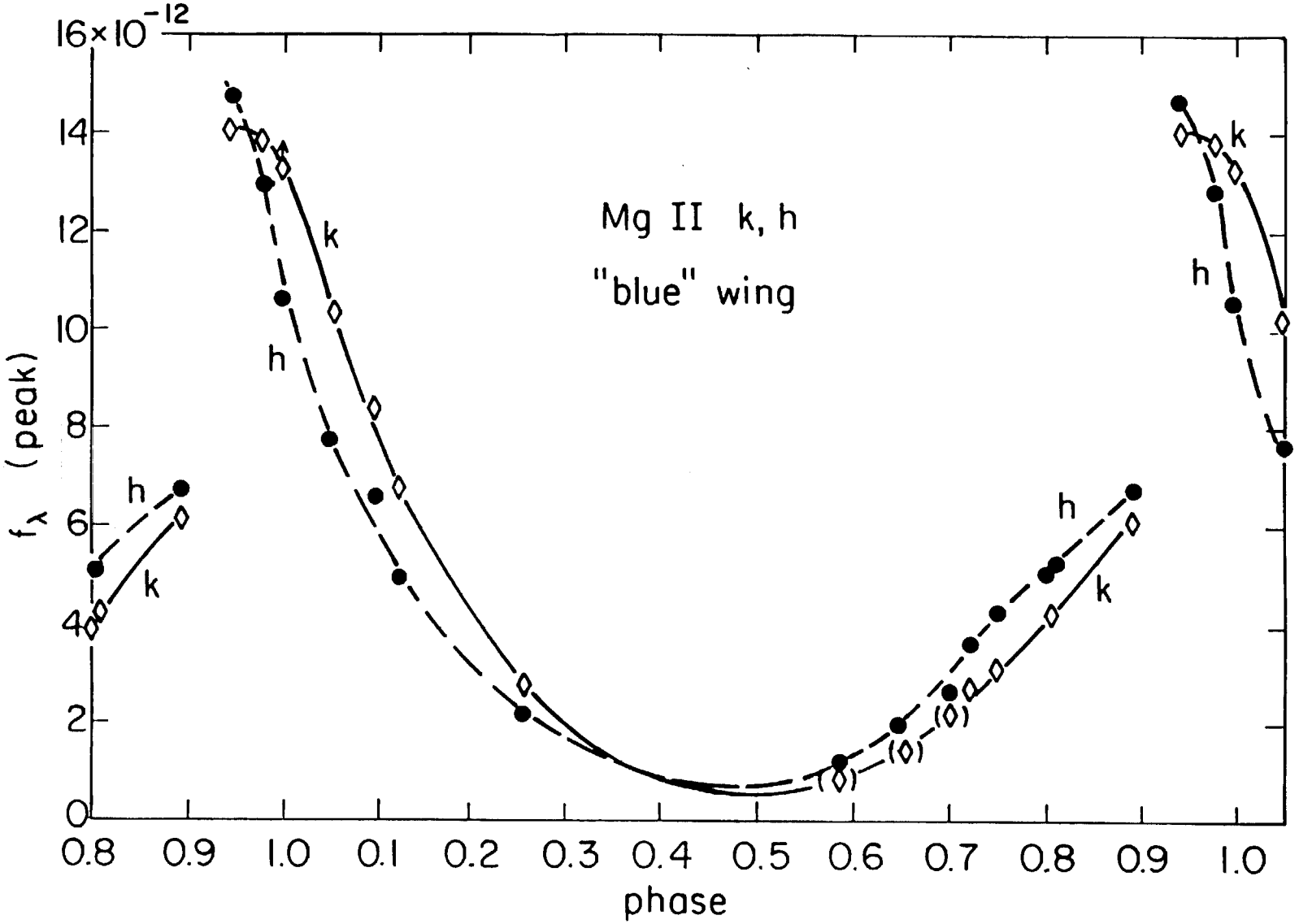

Böhm-Vitense, Lars

Figure 8

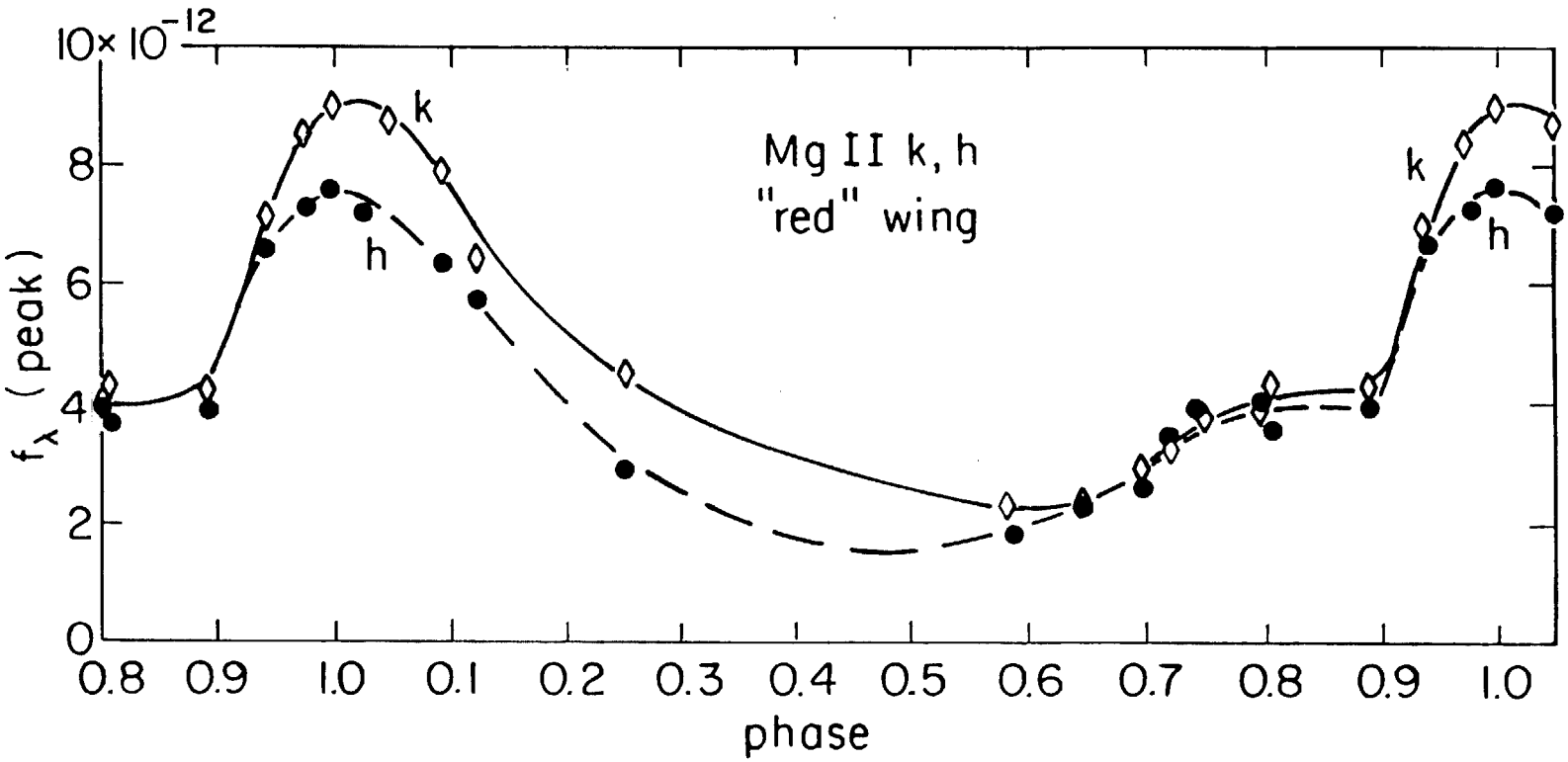

Böhm-Vitense + Love Figure 9

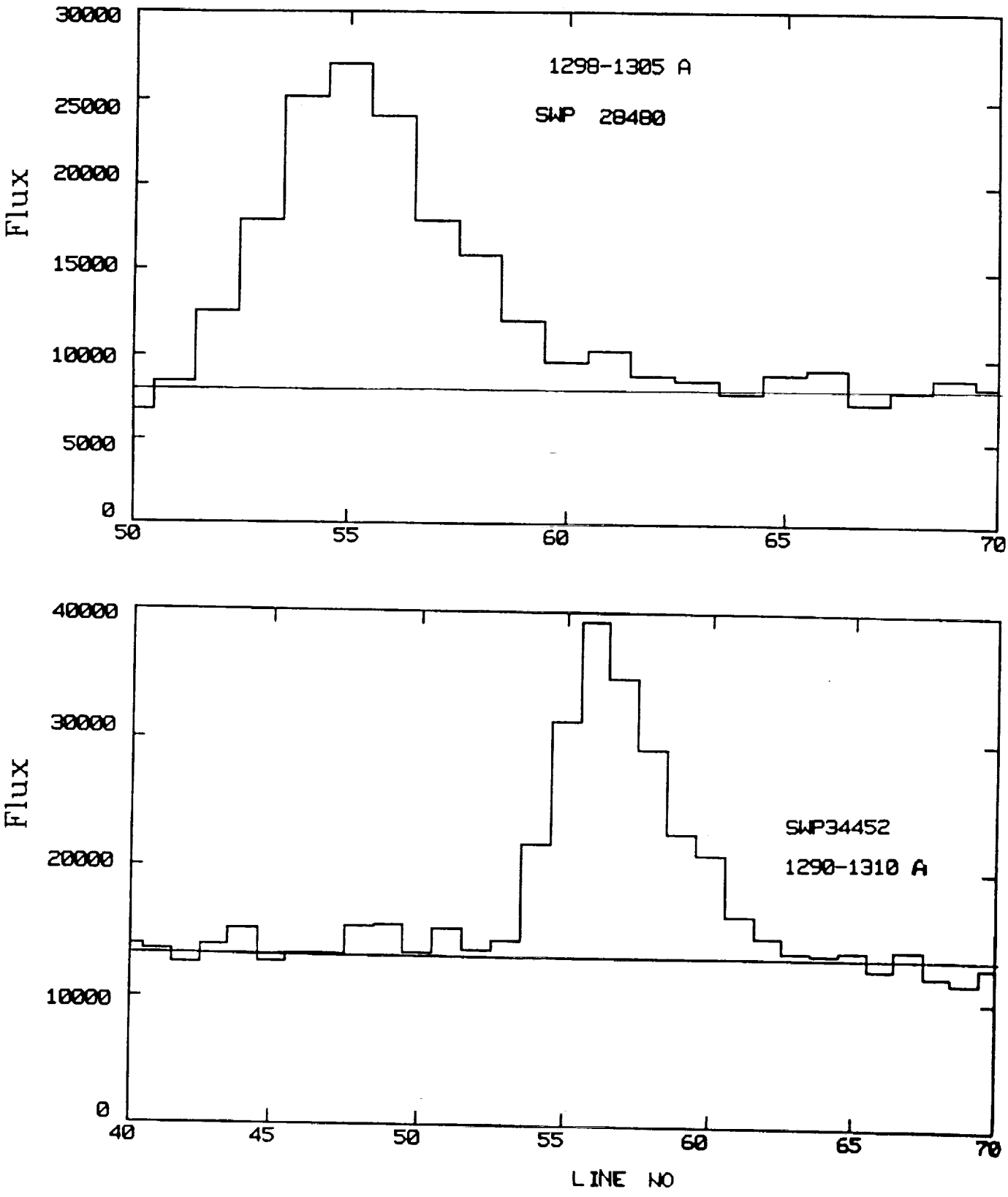

Fig. 10

Böhm - Vilenze and Love

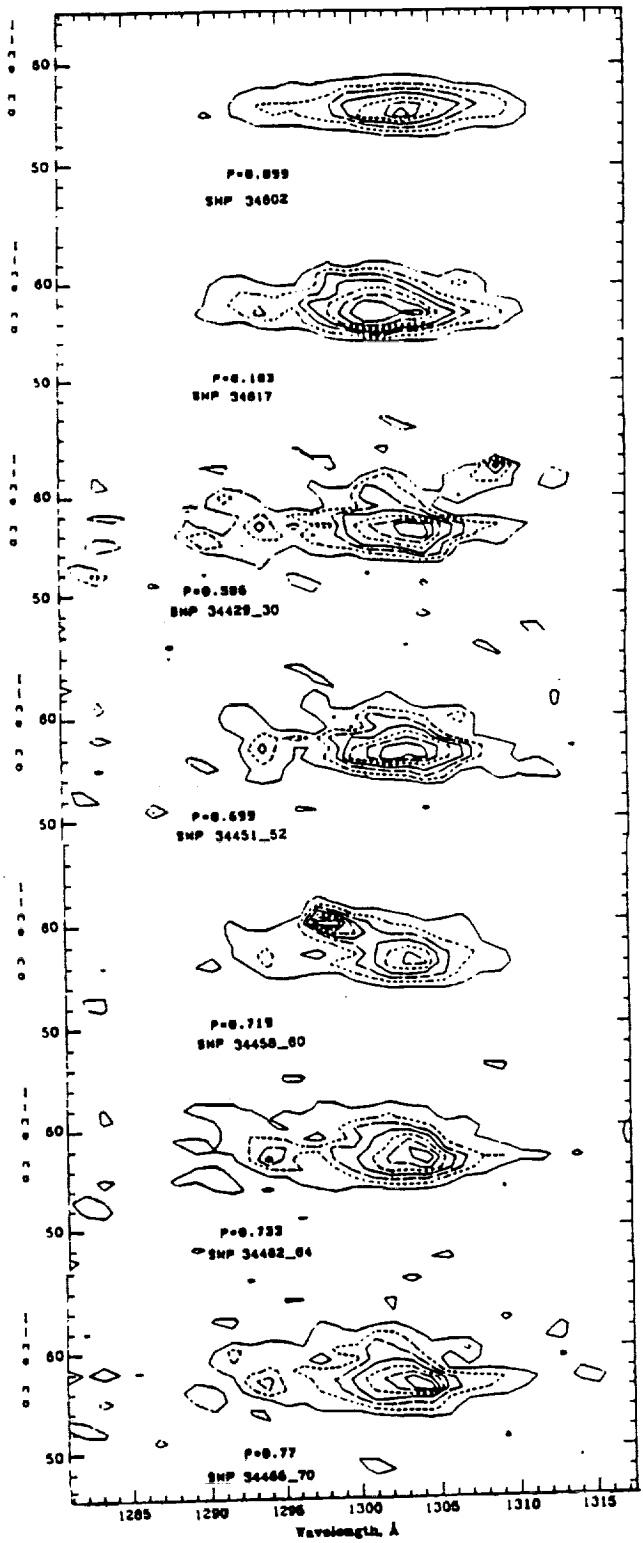

Fig 11

Nelson - Viteuse + Love

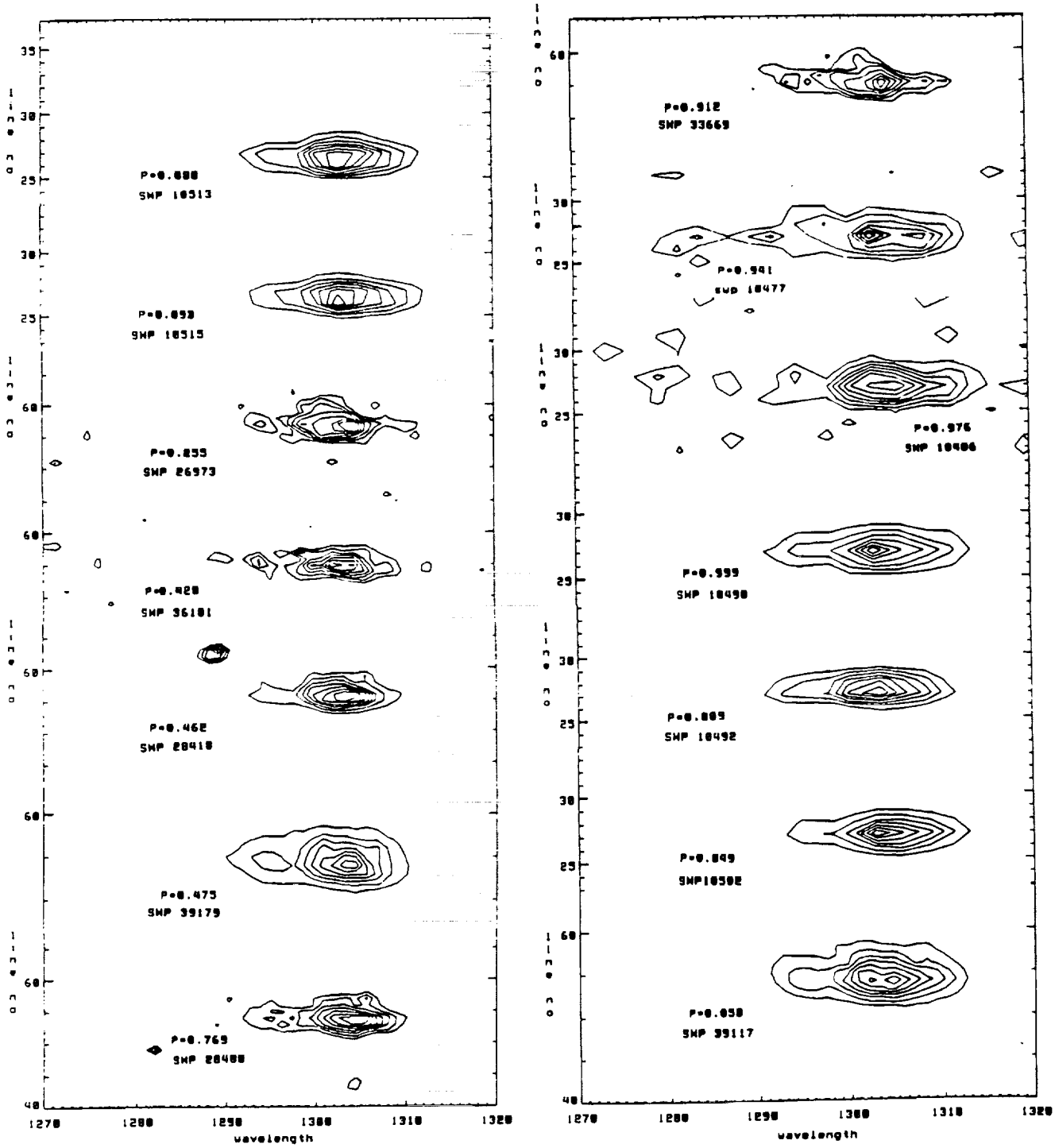

Böhm-Vitense + Love

Fig 12

Böhm-Vitense+Love Fig. 13

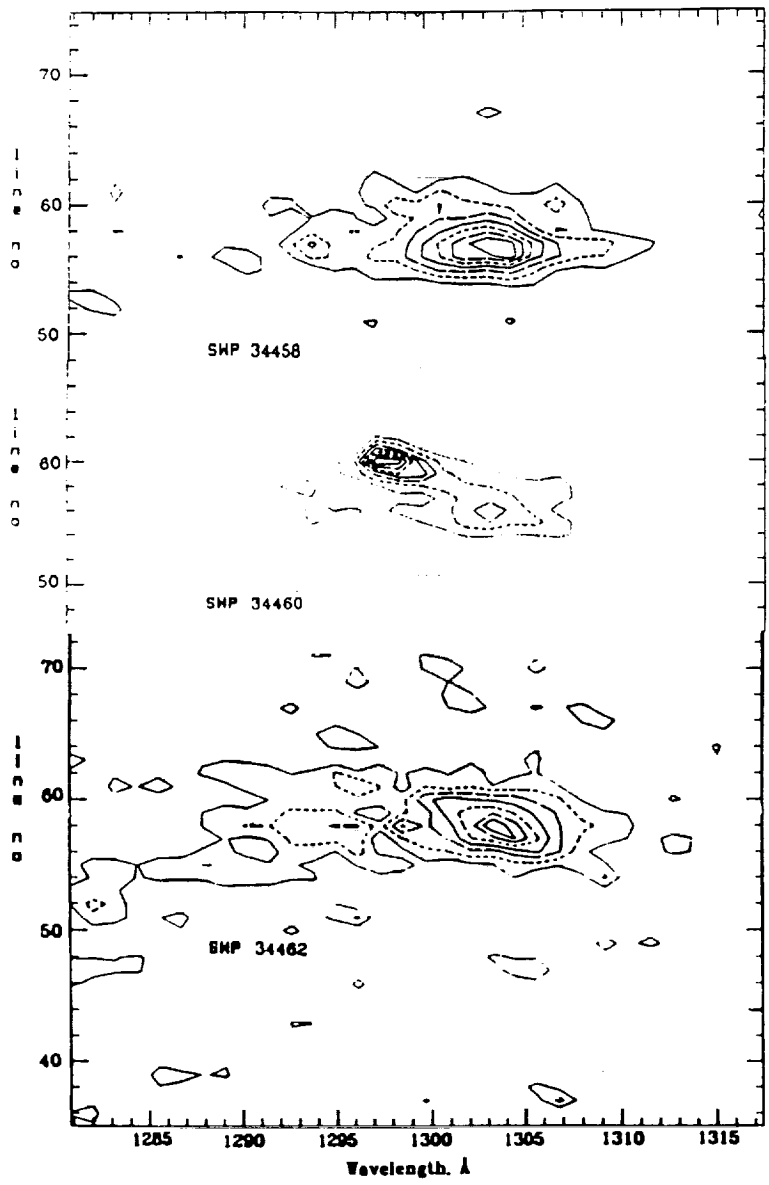

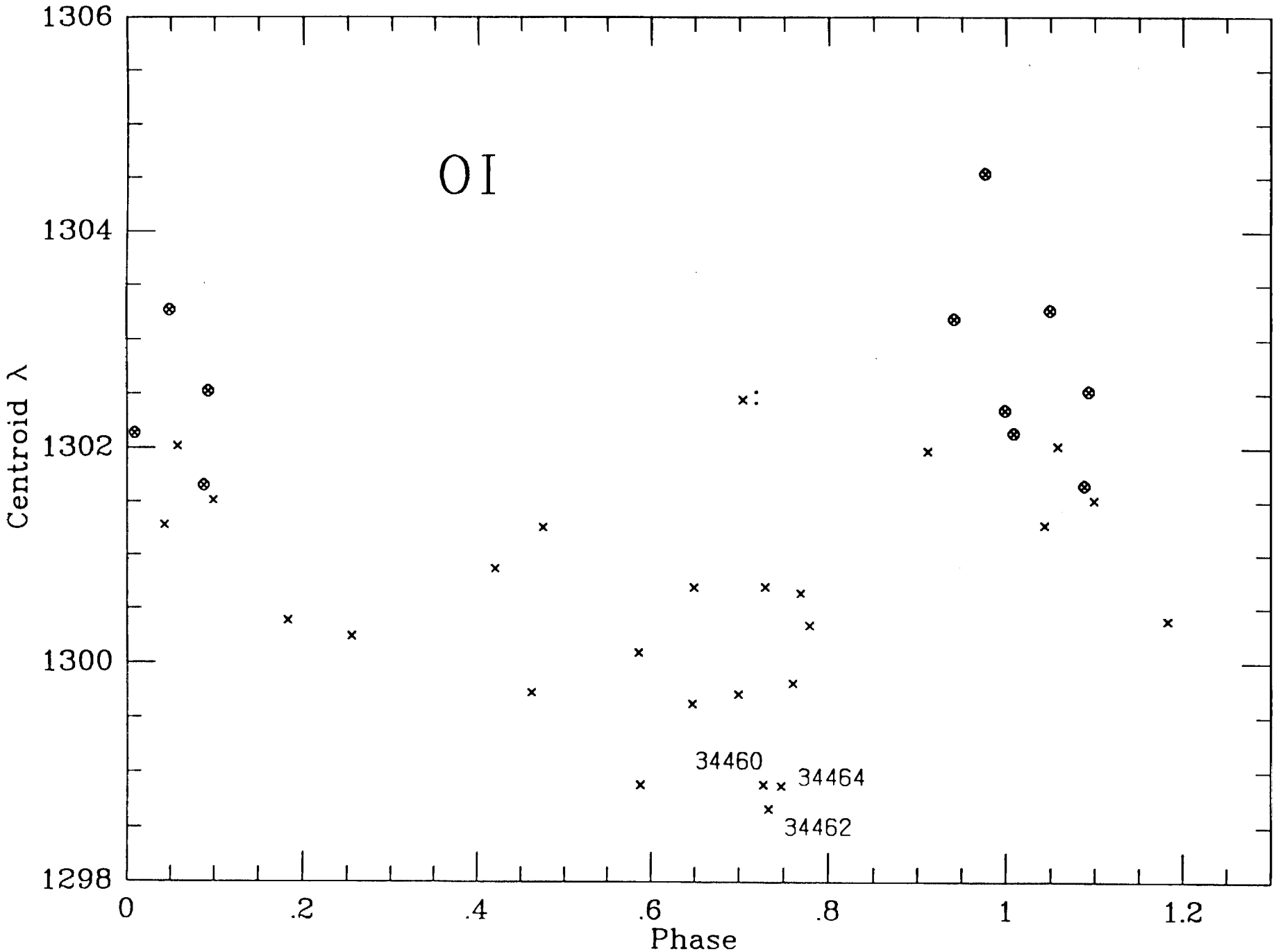

Böhm-Vitense + Love Fig 14

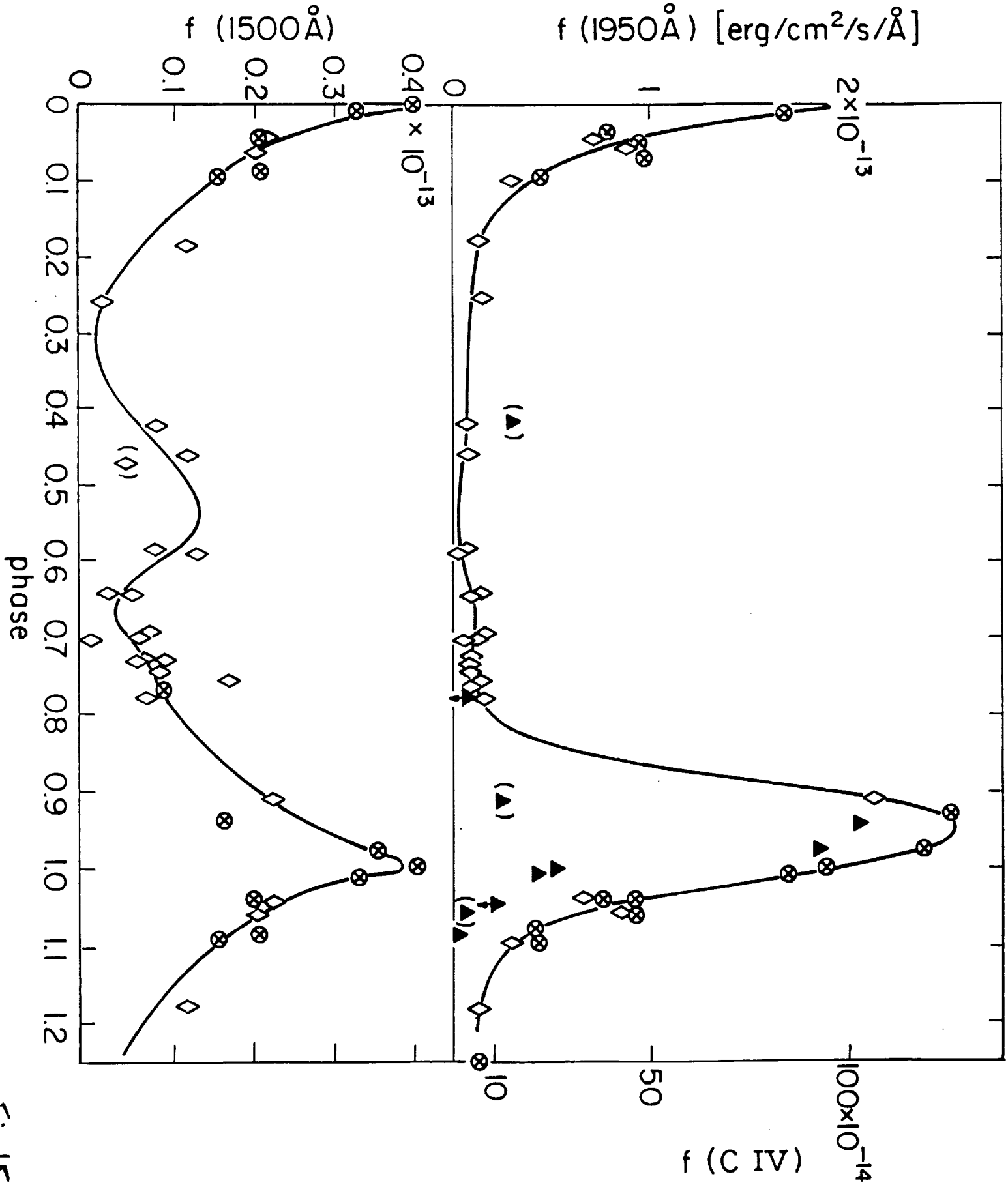

Fig. 15

Böhm-Vitense + Love

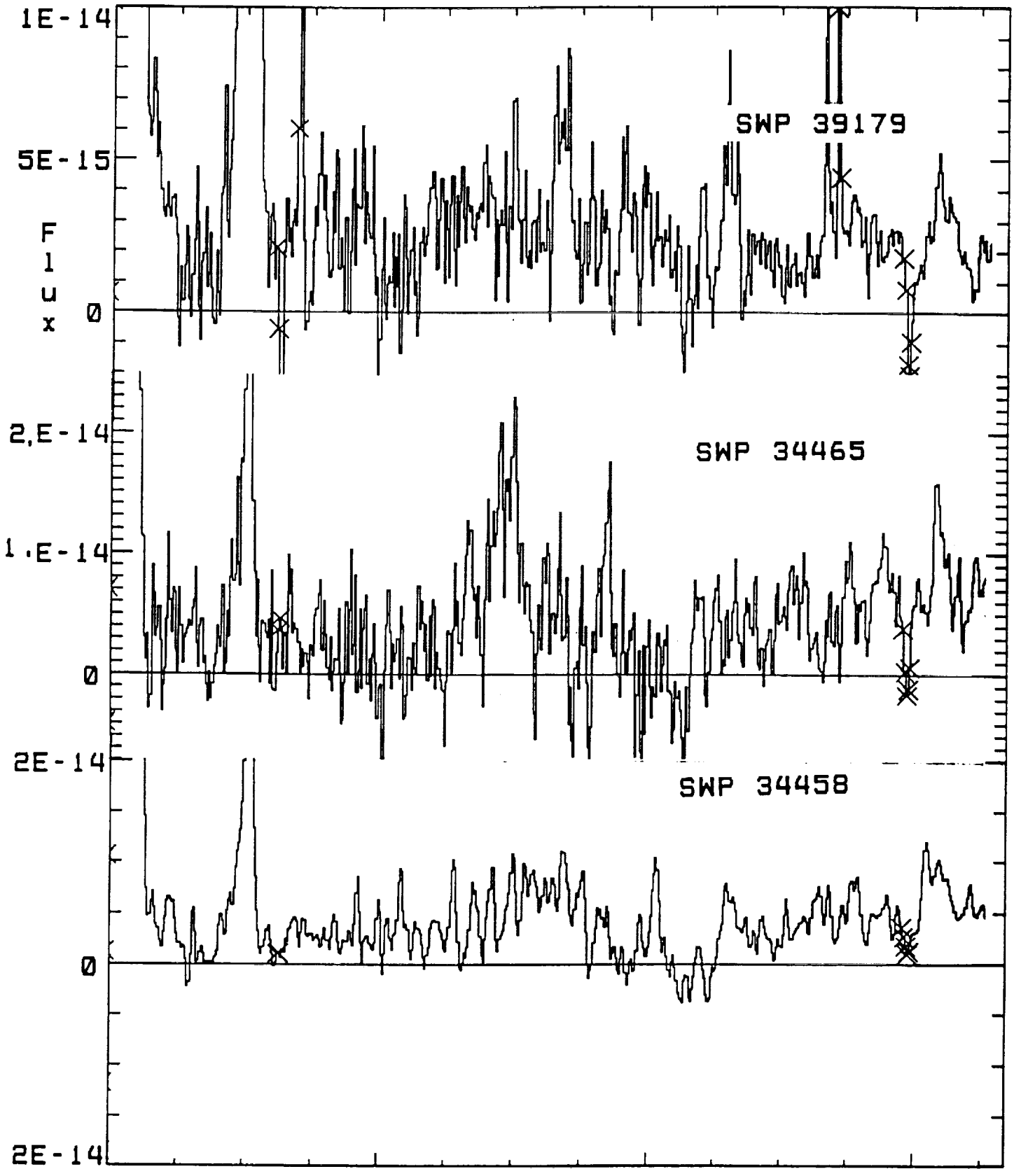
1E-14
5E-15
Flux
0
SWP 39179
2.E-14
1.E-14
0
SWP 34465
2E-14
0
SWP 34458
2E-14
1200
1400
1600
1800
Wavelength

Fig 16

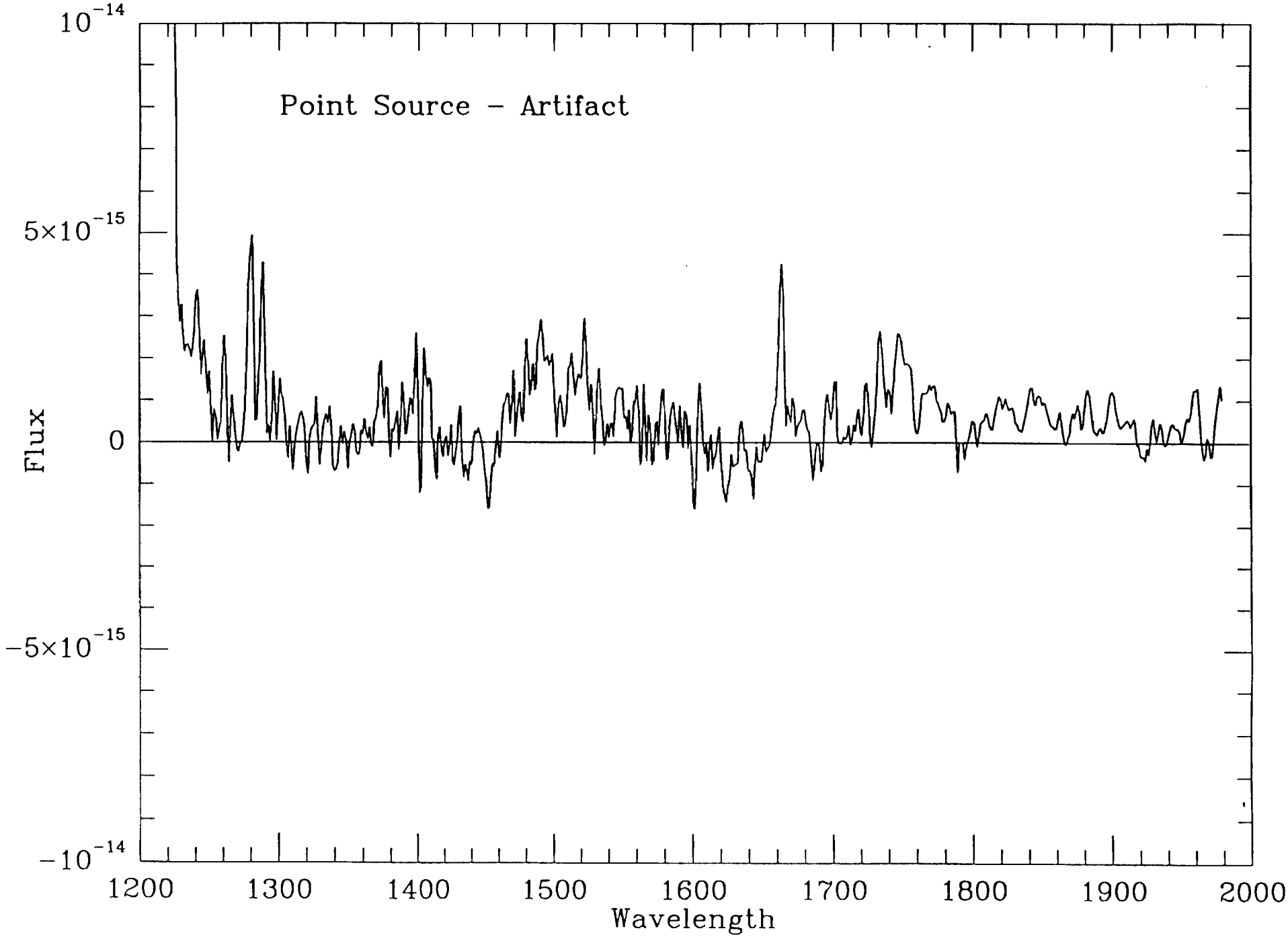

Böhm-Vitense + Love Figure 17